Precambrian Research 384 (2023) 106937

Contents lists available at ScienceDirect

Precambrian Research

journal homepage: www.elsevier.com/locate/precamres

A petroliferous Ediacaran microbial-dominated carbonate reservoir play in the central Sichuan Basin, China: Characteristics and diagenetic evolution

Changwei Li [a], Keyu Liu [a,b,c,*], Jianliang Liu [a,b]

[a] School of Geosciences, China University of Petroleum (East China), Qingdao 266580, China
[b] Key Laboratory of Deep Oil and Gas (China University of Petroleum (East China)), Qingdao 266580, China
[c] Laboratory for Marine Mineral Resources, Qingdao National Laboratory for Marine Science and Technology, Qingdao 266071, China

ARTICLE INFO

Keywords:
Microbial-dominated dolomite
Diagenetic sequence
Favorable reservoirs
Ediacaran Dengying Formation
Sichuan Basin

ABSTRACT

Some of the largest gas accumulations in the central Sichuan Basin, south China are hosted in the Ediacaran microbial-dominated dolomite reservoirs. However, recent exploration of the Secondary Member of the Ediacaran Dengying Formation (Z_2dn^2) has been hampered by an overall lack of understanding of the microbial-dominated dolomite reservoir and its diagenetic evolution process due to its prolonged burial history and complex diagenetic alternation. On the basis of detailed petrographic and geochemical analysis, we have conducted an in-depth investigation on the characteristics, diagenetic sequence and pore evolution process of the microbial-dominated dolomite reservoirs. The main reservoir comprises thromatolitic dolomite, stromatolitic dolomite and straticulate dolomite. Five generations of cement are identified in the microbial dolomite lithofacies. Multiple dissolution, cementation, differential dolomitization, recrystallization and silicification are recognized. Based on elemental geochemistry, carbon and oxygen isotope characteristics, as well as fluid inclusion homogenization temperatures, cements are attributed to six diagenetic stages. The coupling of high-energy deposition, early supergene karsting and dolomitization processes are found to be essential for developing some world-class favorable high-quality microbial-dominated dolomite reservoirs in Z_2dn^2 in the central Sichuan Basin.

1. Introduction

The first occurrence of microbial-dominated carbonate or microbialites can be traced back to 3.5 Ga as microbes and other organisms evolved and earth-surface environments altered (Riding, 2000). Increasing microbialite-related reservoirs of various geological ages have been discovered in recent decades (Table 1). Different from the diverse carbonate sediments in the Phanerozoic, microorganisms, especially cyanobacteria, dominated the carbonate deposition in the Precambrian (Riding, 2006). Therefore, reservoirs in Precambrian strata are almost all related to microbialites, including debris of microbialites deposited in high-energy platform margin. As the search for oil and gas entering towards more deep and ancient strata, an increasing number of microbialite-related reservoirs have been discovered in recent years in China, especially in the Sichuan Basin and the Tarim Basin. However, when studying microbialite reservoirs, geologists often neglect the differences among various microbialite reservoirs, their distinct diagenetic sequences and pores evolution process compared with non-microbialite reservoirs.

Although enormous amount research work has been done on the diagenetic and pores evolution of microbialites in Sichuan Basin, the accurate and detailed diagenetic sequence of microbialite reservoirs are still in a state of some disarray, because of the lack of targeted research on microbialite reservoirs by using the combination of petrophysical and geochemical evidences. Wang (2000) recognized three periods of cementation and fourth geochemical precipitates in Sinian dolomites in Southwest Sichuan. Then Li (2009) divided the diagenetic stages into syngenetic, eogenetic, telodiagenetic and superegenetic periods. And Peng (2010) found three stages of cementation and two period's silicification in Sinian dolomites in Southeast Sichuan. Meanwhile Shi (2010) and Wang (2010) established the diagenetic sequence of Dengying Formation respectively. Wang (2011) considered the dolomite cements formed in four peroids: penecontemporaneous periods, supergenetic periods, shallow burial periods and deep burial periods. By using cathode luminescence and trace elements, Shi (2013) recognized five periods of dolomite cements in Dengying microbialites in Southeast Sichuan

* Corresponding author at: School of Geosciences, China University of Petroleum (East China), Qingdao 266580, China.
E-mail addresses: Rockleea@163.com (C. Li), liukeyu@upc.edu.cn (K. Liu).

https://doi.org/10.1016/j.precamres.2022.106937
Received 4 June 2022; Received in revised form 29 November 2022; Accepted 29 November 2022
Available online 15 December 2022

Basin. By reservoirs research based on field outcrops and wells, Zhu (2015) reconstructed the diagenetic sequence of Dengying Formation in Sichuan Basin. Hu (2020) recovered the dolomitization history and porosity evolution of Dengying Formation and identified four stages of dolomites as well as quartz and bitumen.

2. Geological setting

Our study area is located in the central Sichuan Basin, the Upper Yangtze Platform (Fig. 1A, B) covering an area of 195 km long (E-W) and 115 km wide (N-S). It is delineated by four exploration wells: the MX26 (north), MX23 (east), P1 (south) and GS1 (west) wells. During the Ediacaran, the Upper Yangtze Platform was located at approximately 30 °N latitude under a weak extensional tectonic setting (Wang et al., 2003) as a result of the breakup of the Pannotia supercontinent (Christopher, 2009). On the basis of lithological variations, the Ediacaran Dengying Formation can be subdivided into four members from the bottom to the top (Fig. 1C), namely, Z_2dn^1, Z_2dn^2, Z_2dn^3 and Z_2dn^4, respectively (Li et al., 2013). The underlying the Doushantuo Formation, which is composed of sandstone and dolomicrite with minor gypsolyte as revealed in Well W117, was developed in an evaporative lagoonal environment (Liu et al., 2015). The lithology in Z_2dn^1 is composed mainly of light-gray to dark-gray lamellar dolomicrite and silty dolomite, which are interpreted to have been deposited in a semi-restricted carbonate platform (Hu et al., 2019). The Z_2dn^2 strata unit, dominated by stromatolites and thrombolites with botryoidal structures, was deposited in a restricted, rimmed carbonate platform environment (Zhao et al., 2016). Rapid marine transgression resulted in a rapid depositional accommodation increase, leading to the deposition of Z_2dn^3, which was dominated by blue-gray to dark-gray mudstones in the central Sichuan Basin (Li et al., 2014). With a gradual regression and oscillations of the sea level, microbialites along with granular dolomites became dominated in the rimmed platform in Z_2dn^4 (Zhao et al., 2020). The Lower Cambrian Maidiping Formation or Qingzhusi Formation unconformably capped on Z_2dn^4 as a result of the Tongwan II movement (Zhou et al., 2020).

During the Late Ediacaran, an aulacogen was developed in the central Sichuan Basin (Fig. 1D; Du et al., 2016), providing a favorable tectonic and paleo-geographic setting for the deposition and development of microbial-dominated carbonate reservoirs. Although geologists share different opinions about the origin of the aulacogen, stratigraphic forward modeling indicated that the Dengying Formation was developed within the aulacogen under an overall extensional tectonic setting and in response to global eustacy (Liu et al., 2020). The second member of the Dengying Formation (Z_2dn^2) was deposited during the initial phase of expansion of the trough, during which thick fast-growing microbialites developed near the margin forming extensive carbonate platform facies with relatively thin carbonate deposition within the trough. The Z_2dn^2 carbonate platform was subsequently uplifted and had been partially eroded during the first episode of the Tongwan movement (Wang et al., 2014). Afterwards, widespread marine transgression led to the deposition of mixed carbonate and clastics during the deposition of the third member of the Dengying Formation (Z_2dn^3; Ma et al., 2019) and a thick microbialite succession in the platform during the deposition of the fourth member of the Dengying Formation (Z_2dn^4; Li et al., 2018) in the aulacogen. This was followed by the second episode of the Tongwan movement which resulted in the uplifting of the entire Upper Yangtze Craton. Z_2dn^3 and Z_2dn^4 experienced widespread erosion, locally the denudation even reached down to Z_2dn^2 in the Weiyuan-Ziyang area (Xu et al., 2012). The tectono-sedimentary evolution had exerted a profound impact on the reservoir diagenetic evolution of the second member of the Dengying Formation.

3. Materials and methods

A total of 126 samples were collected from 10 wells (Appendix 1), with depth varying from 5522 m to 3024 m in the paleo-uplift region in the central Sichuan Basin. Petrographic thin sections were made on all samples. Fifty samples were prepared by vacuum impregnation with blue epoxy resin to highlight pore spaces. Sixty samples were sliced to 100 μm thick sections for fluid inclusion observation. Sixty-seven samples were sliced to 500 μm thick sections for cathode luminescence (CL) observation and in situ cement sampling via micro-drilling. Electronic microprobe analysis was performed on different phases of cementation of three microbialite samples with up to 45 points to obtain their major and minor elements abundances. Cements formed in different diagenetic phases delineated by CL analysis in 8 samples (thick sections) were sampled via micro-drilling for isotope analysis. Up to 42 sets of carbon and oxygen isotope data were acquired from those micro-drilling samples. More than 128 groups of fluid inclusion in different generations of cement were measured to obtain homogenization temperatures from 34 samples.

Table 1
Lithological and sedimentary facies characteristics of diverse microbial-dominated reservoirs reported worldwide.

Stratigraphic interval	Region	Main reservoir lithology	Sedimentary facies	References
Mesoproterozoic Wumishan Fm	Bohaiwan Basin, China	Stromatolitic and thrombolitic dolomites	Subtidal and intertidal in ramp	Fei et al., 2005; Lu et al., 2021
Upper Vendian (Late Proterozoic)	Siberian Platform, Russia	Stromatolitic dolomites and sandstones	Tidal-flat in ramp	Melnikov, 2008; Shemin et al., 2012
Upper Ediacaran Dengying Fm	Sichuan Basin, China	Thrombolitic and microbial foam dolomites	Rimmed carbonate platform	Wang et al., 2016; Liu et al., 2016
Upper Ediacaran Qigebulake Fm	Tarim Basin, China	Stromatolitic dolomites	Restricted platform	Shi et al., 2017; Hu et al., 2021
Ediacaran-Early Cambrian Ara Group	Salt Basin, South Oman	Stromatolites, carbonate laminites	Restricted middle and inner ramp	Stefan et al., 2005; Grotzinger et al., 2014
Lower Cambrian Xiaoerbulak Fm	Tarim Basin, China	Thrombolitic and stromatolitic dolomites	Inner and middle ramp	Song et al., 2014; Deng et al., 2018
Middle Ordovician Majiagou Fm	Ordos Basin, China	Strombolitic dolomites	Shallow platform	Xie et al., 2020
Latest Visean and Serpukhovian stages	Caspian Basin, Kazakhstan	Micrite-cement boundstones	Margin and slope of isolated platform	Kenter et al., 2005; Ana et al., 2021
Late Permian Stassfurt Fm	Netherlands, Denmark & Poland	Stromatolitic and thrombolitic dolomites	Supratidal to subtidal in platform	Słowakiewicz et al., 2013; Tone, et al., 2018
Middle Triassic Leikoupo Fm	Sichuan Basin, China	Thrombolitic and stromatolitic dolomites	Restricted carbonate platform	Liu et al., 2016; Duan et al., 2021
Upper Jurassic Smackover Fm	Alabama, USA	Thrombilitic boundstone, microbial buildups	Subtidal in an inner ramp	Haddad et al., 2013
Lower Cretaceous Barra Velha Fm	Santos Basin, Brazil	Stromatolites, spherulatites and laminites	Shallow alkaline lacustrine	Marcos et al., 2009; Bruno et al., 2019
Eocene Green River Fm	Utah, USA	Stromatolites, thrombolites and grainstones	Marginal lacustrine	Frantz et al., 2014; Thomas et al., 2015;

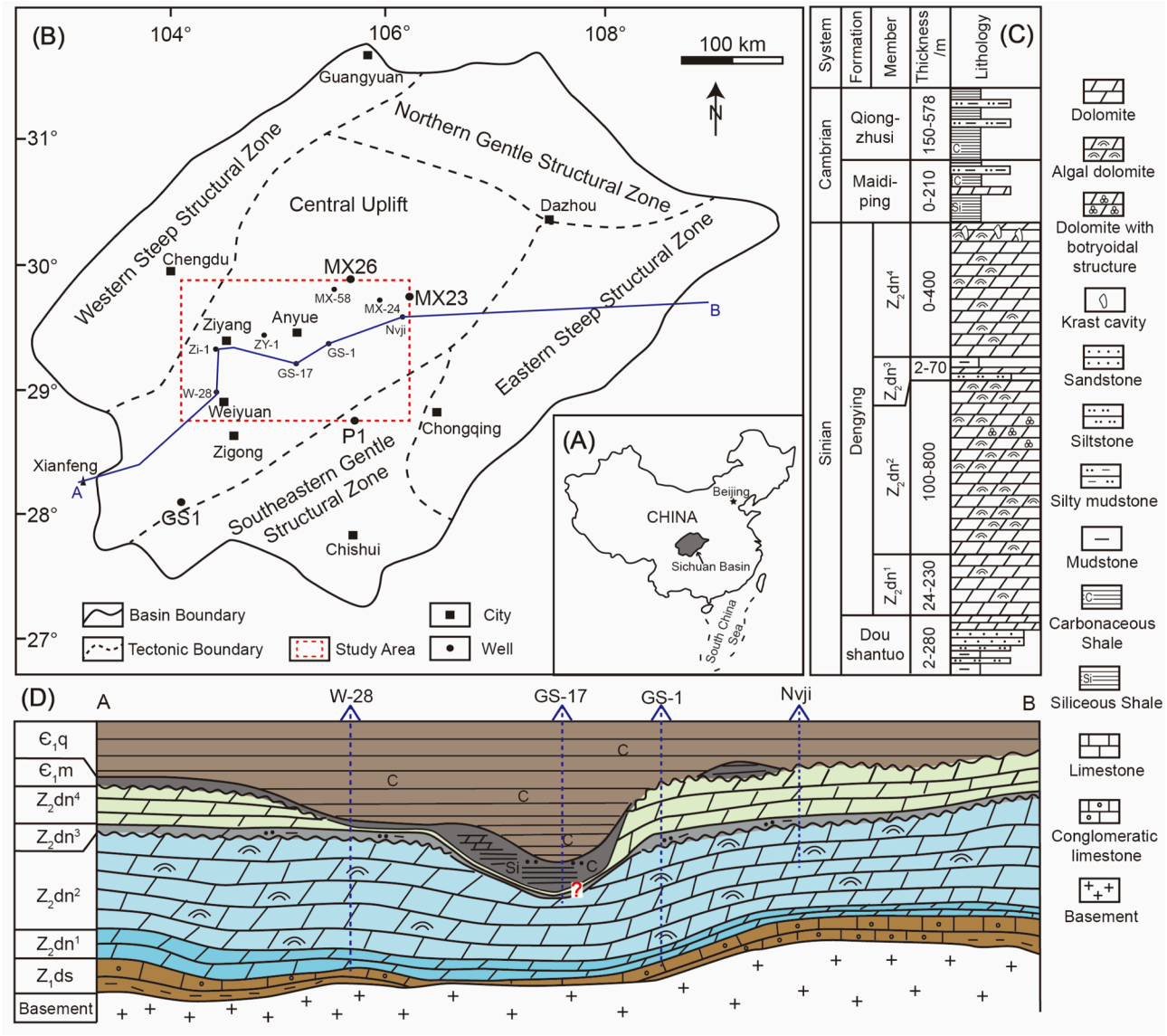

Fig. 1. (A) Location of the Sichuan Basin. (B) Major tectonic and structural units of the Sichuan Basin with the location of the study area shown. (C) Generalized stratigraphic column of the Ediacaran and Lower Cambrian periods, showing lithologies and depositional thicknesses of each member. (D) A near E-W lithofacies profile flattening to the Cambrian Qiongzhusi Formation, showing lithofacies and thickness difference within and outside the aulacogen. Location of the A-B profile is shown in Fig. 1B (after Liu et al., 2020).

4. Results

4.1. Petrology

Detailed core observation and microscopic characterization indicate that the microbial dolomite reservoirs in the Dengying Formation consist mainly of stromatolitic dolomites, thrombolitic dolomites and straticulate dolomites.

Thrombolites refers to microbialites that have macroscopically clotted fabrics (Riding, 2000). Microscopic observation indicates that microclots in the Dengying Formation were originally formed by dark microbial agglomerations of dolomicrite. There are two categories of thrombolitic dolomites, namely rimmed thrombolitic dolomites and granular-related thrombolitic dolomites, respectively. The rimmed thrombolitic dolomites display an equal-thickness straticulate rim around the cryptocrystalline cores (Fig. 2A). The rim usually comprises more than one eccentric cements with thickness varying from several to a dozen centimeters. The inner core is composed mainly of amorphous microclots with diameters ranging from 2 mm to 15 mm (Fig. 2B). It may have developed in a relative high-energy setting in the platform interior (Yang et al., 2020). The granular-related thrombolitic dolomites are generally imbedded within grainstone and are characterized by elliptic microclots (Fig. 2C). Thin rims can sometimes be observed around clots but their thicknesses are much smaller than the clots. The inner part of microclots were recrystallized, filled by cryptal dolomite debris or replaced by sparry cements (Fig. 2D). Those evidence suggests the granular-related thrombolytic dolomites were developed in a high-energy, lower subtidal zone of the platform margin (Lan et al., 2019).

The stromatolitic dolomites is characterized by distinct undulant-columnar shapes and internal consecutive alternation of dark and light laminae (Fig. 2E). The stromatolitic dolomites is composed of dark-laminae dolomite rich in organic matters and light-laminae dolomite rich in crystalline dolomite debris (Fig. 2F). The dark laminae are generally 0.1–0.3 mm in thickness, whereas the thickness of the light laminae can vary from 0.2 mm to1.5 mm approximately (Fig. 2G). Previous research demonstrated that stromatolitic dolomites, distinguished by their macroscopic morphology and cumulative thickness, may be formed in the lower intertidal or upper subtidal zones of the

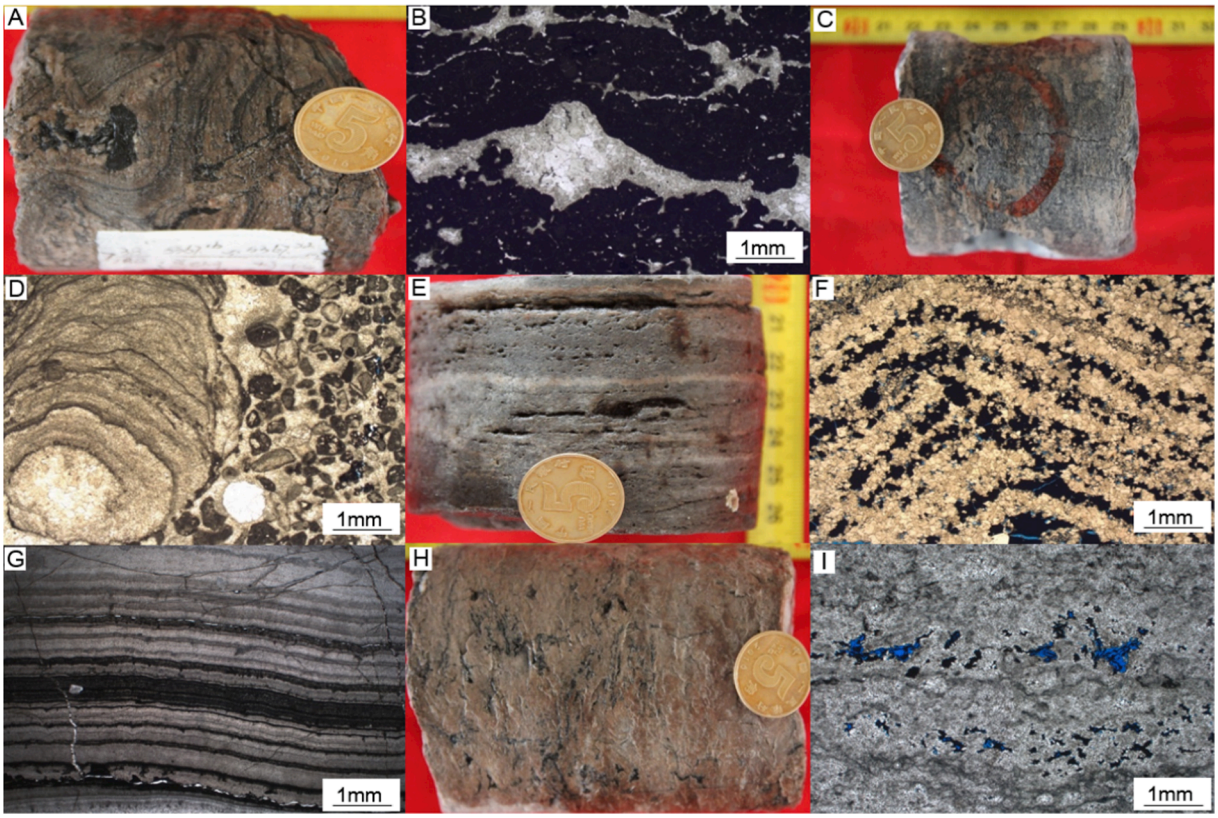

Fig. 2. Petrologic characteristics of different microbial dolomites in Z_2dn^2. (A) thromatolitic dolomites type I, microbial debris encircled by isopachous cements; (B) thromatolitic dolomites type I, irregular dolomicrite microclots cemented by multiple dolosparite; (C) thromatolitic dolomites type II, dark dolomicrite microclots and dolosparite cements have distinct boundary; (D) thromatolitic dolomites type II, microclots accompanied with sandy dolomite; (E) stromatolitic dolomites show alternation of parallel dark lamina and light lamina; (F) stromatolitic dolomites with well-developed stratiform dissolution pores and bitumen filling; (G) stromatolitic dolomites devoid of valid pores; (H) straticulate dolomites with sparse microbial lamina; (I) elongated dissolution pores generated between microbial lamina in straticulate dolomites;

platform interior or platform margin in the Dengying Formation (Hu et al., 2019).

Straticulate dolomites are defined as a discontinuous straticulate benthic cyanobacteria deposit that are often interbedded with dolomicrite or fine-crystalline dolomite. The dark cyanobacteria deposit is sparsely distributed in dense dolomicrite or fine-crystalline dolomite (Fig. 2H). The microbial component can generally be wrinkly stretched or twisted together to form microclot-like fabrics (Fig. 2I). The presence of predominant bird's-eye pores implies that this lithology may have been deposited in a relative shallow-water environment compared with the stromatolitic and thrombolitic dolomites.

4.2. Interstitial impurity

Different microbialite reservoirs of Z_2dn^2 in the central Sichuan Basin are filled by different phases of carbonate cement, quartz and bitumen. Based on photomicrograph analysis and cathode luminescence (CL) observation, we recognized five generations of cement in the microbialite reservoirs (Fig. 3A, E). The host rock usually presents a dull-red luminescence under CL, which usually becomes light-red luminescence after recrystallization (RH) (Fig. 3A, B). The first generation of cement (Cd1) usually show yellowish CL color and distributed around microclots in thrombolitic dolomites or dark laminae in stromatolitic dolomites and straticulate dolomites (Fig. 3A, C). The cement is often characterized by a fibrous texture with the idiomorphic monocrystal major axis shorter than 0.05 mm. The second generation of cement (Cd2) displays an dull-red CL color, and often infills in dissolution pores, vugs and fibrous cements (Fig. 3A, C). This cement is characterized by multiple isopachous layers, which can form botryoidal structures in thrombolitic dolomites and stromatolitic dolomites. The third generation of cement (Cd3) is characterized by an orange CL color and foliated dolomite with a xenomorphic to subhedral monocrystal major axis ranging from 0.05 mm to 0.25 mm (Fig. 3A, D). The fourth generation of cement (Cd4) is characterized by clean and transparent dolomites with yellow CL color and an idiomorphic monocrystal major axis larger than 0.25 mm (Fig. 3A, D). Dolomite crystals in the fifth generation of cement (Cd5) are mostly of curved to saddle-like appearance and bright yellow CL color (Fig. 3E, F). They are believed to have been generated by hydrothermal fluid (Jiang et al., 2016), along with minor subhedral quartz (Q) in stromatolitic dolomites and straticulate dolomites.

4.3. Reservoir storage space characteristics:

Detailed core observation and thin section identification indicate that most primary pores have been cemented or modified with secondary pores being the predominant type in the Dengying Formation. According to the pore classification scheme of Choquette and Pray (1970), and Lønøy (2006), six types of reservoir storage space are identified in Z_2dn^2, including residual microbial framework pores, enlarged interclot pores, intraclot dissolution pores, stratiform dissolution pores, vugs, minor moldic pores and fractures (Fig. 4).

Residual dissolved microbial framework pores are formed by dissolution but partially filled by cements, which are mainly developed in thromatolitic dolomites and stromatolitic dolomites (Fig. 4A). Enlarged Interclot and intraclot pores are pervasively developed in clot-related thromatolitic dolomites (Fig. 4B, C). Stratiform dissolution pores are characteristic pores in stromatolitic dolomites and straticulate dolomites (Fig. 4D). Dissolution vugs are formed during the supergene period and

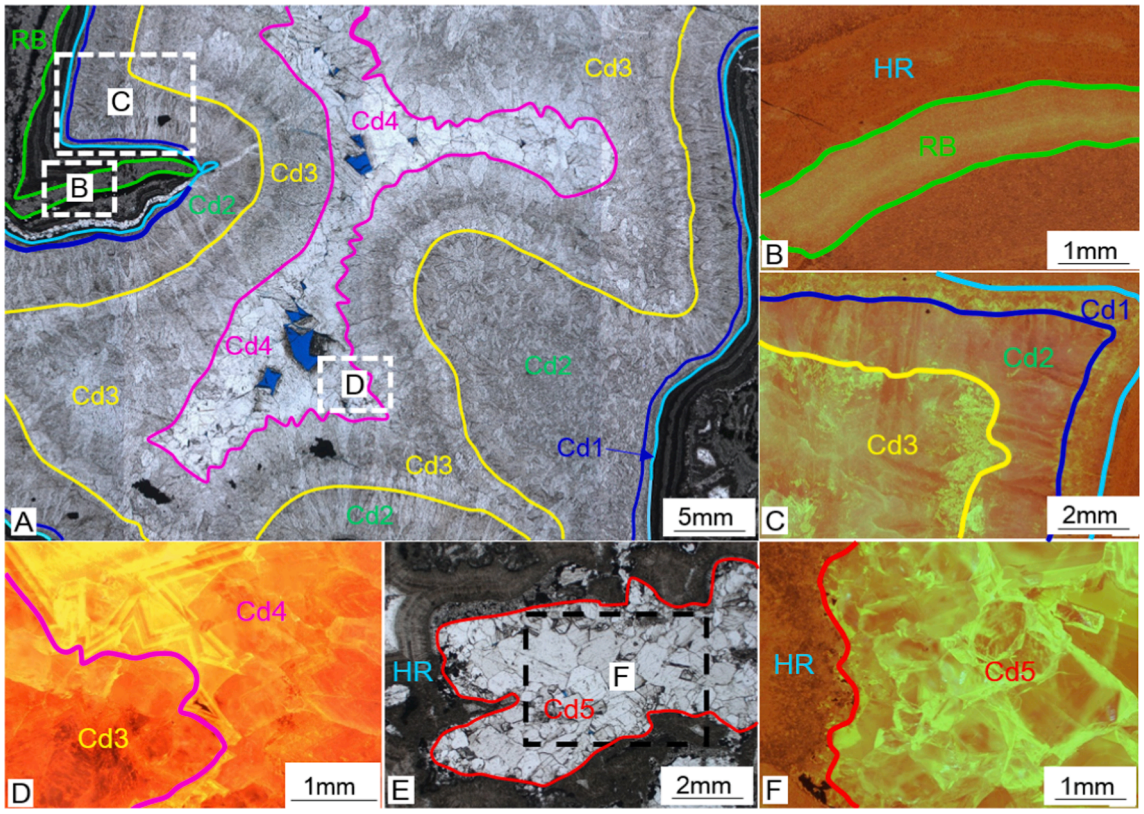

Fig. 3. Petrologic and cathode luminescence (CL) characteristics of five generations of cement in different microbial dolomites in Z_2dn^2. (A) Four generations of cements in microbialites, isopachous dolomites growing on fibrous dolomites and followed by silty-fine crystalline dolomites , then medium-coarse crystalline dolomites located in the central part of vugs; (B) Dull-red CL of host rock and light-red CL after recrystallized; (C) Yellowish CL of Cd1, dull-red CL of Cd2 and orange CL of Cd3; (D) Orange CL of Cd3 and yellow CL of Cd4; (E) Saddle-like appearance of Cd5; (F) Bright yellow Cl of Cd5; HR: Host Rock; (For interpretation of the references to color in this figure legend, the reader is referred to the web version of this article.)

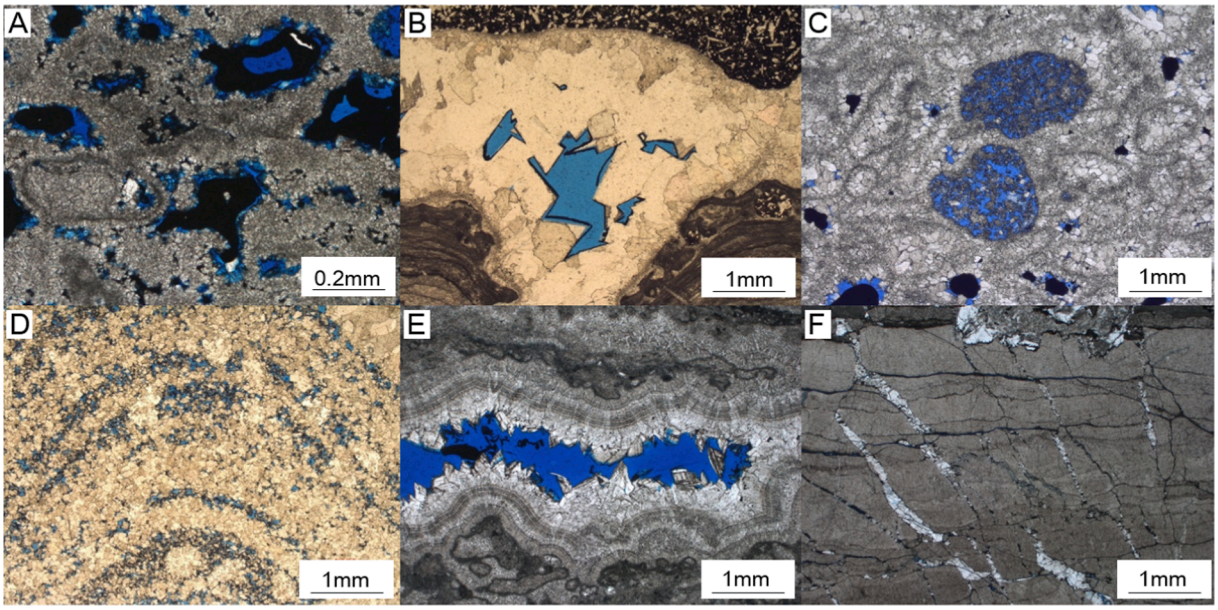

Fig. 4. Microscopic characteristics of six pore types in different microbialitic dolomites in Z_2dn^2. (A) Residual microbial framework pores; (B) Enlarged interclot pores; (C) Moldic pores; (D) Stratiform pores; (E) Vugs; (F) deep burial pores with fractures;

can be developed in all three microbialites (Fig. 4E). Although fractures can improve permeability, it would have minor influence on the total porosity in the Dengying Formation (Fig. 4F), which were thus not discussed in this paper.

4.4. Geochemical characteristics

4.4.1. Elemental analysis

The contents of the major elements of the 45 points in different

textures of microbialites measured by EPMA (electron microprobe analysis) are listed in Appendix 2. A minor discrepancy of ω(MgO) and ω(CaO) can be seen in three different microbialites dolomites. The values of ω(MgO) and ω(CaO) in thrombolitic dolomites vary from 20.04 % to 23.44 % (avg. 21.08 %) and 27.47 % to 31.21 % (avg. 29.53 %), respectively (Table 2), while the ratio of CaO and MgO increase with progressive cementation from RH to Cd1 → Cd5 (Table 3). The values of ω(Na_2O), ω(K_2O) and ω(FeO) decrease, whereas ω(BaO), ω(SrO) and ω(MnO) increase with progressive cementation (Fig. 5).

The stromatolitic dolomites has the lowest MgO contents ranging from 17.71 % to 22.57 % with an average value of 20.49 % and CaO contents range from 21.44 % to 30.61 % with an average value of 28.31 % (Table 2). Except for one data point, the CaO/MgO ratios of different cements increase while the FeO/MnO ratios decrease with increasing burial of the stromatolitic dolomites (Table 3). The values of ω(SrO) and ω(BaO) dramatically increase when the stromatolitic dolomites became silicified (Fig. 5). The value of ω(FeO) decreases in the late-stage cements while ω(MnO) shows an opposite trend (Table 3).

The straticulate dolomites have the highest ω(MgO) and ω(CaO), varying from 20.59 to 22.81 % (avg. 21.58 %) and 28.19 % to 30.62 % (avg. 29.45 %), respectively (Table 2). The CaO/MgO ratio shows an inconspicuous tendency for the cements formed during different periods (Table 3). The ω(BaO) and ω(MnO) values of different cements increase with with progressive cementation or burial, while other minor elements show no particular trend with with progressive cementation or burial (Fig. 5).

In summary, the FeO/MnO ratios decrease gradually with progressive cementation in all three microbialites (Table 3), which is consistent with an increasing CL intensity of cements (Fig. 3) formed later. The CL intensity decrease in the saddle dolomites due to the increasing ratio of ω(FeO) over ω(MnO).

4.4.2. Carbon and oxygen isotope data

As illustrated in Fig. 6, there are apparent variations in the $\delta^{13}C$ and $\delta^{18}O$ ratios among different phases of cement in the eight samples investigated. From Cd1 to Cd5, the $\delta^{13}C$ and $\delta^{18}O$ values become progressively negative (Fig. 6). The carbon and oxygen isotope ratios of different cements appear to be more related to their formation phases rather than their lithologies. The $\delta^{13}C$ and $\delta^{18}O$ ratios of Cd1 and Cd2 are almost the same with $\delta^{13}C$ ratios ranging from 1 ‰ to 2.6 ‰ (avg. 1.7 ‰), and the $\delta^{18}O$ ratios ranging from −6.1 ‰ to −3.2 ‰ (avg. −5.1 ‰). The $\delta^{13}C$ and $\delta^{18}O$ ratios of Cd3 have ranges of 0.4 ‰–1.6 ‰ (avg. 1.1 ‰) and −9.3 ‰ – −7.1 ‰ (avg. −8.1 ‰), respectively. The $\delta^{13}C$ and $\delta^{18}O$ ratios of Cd4 range from 0.6 ‰ to 1.1 ‰ (avg. 0.9 ‰) and −11.8 ‰ to −11.7 ‰ (avg. −11.7 ‰), respectively. Cd5 has the most negative $\delta^{13}C$ ratio of −1‰ to −0.6 ‰ (avg. −0.8 ‰), and $\delta^{18}O$ ratios between −10.7 ‰ and −9.3 ‰ (avg. −10.0 ‰).

4.4.3. Homogenization temperatures (Th) of fluid inclusions

There are quite abundant primary two-phase (liquid–vapor) fluid inclusions in the dolomite cement. After eliminate these re-equilibrated fluid inclusions, at least three inclusions from each fluid inclusion assemblage are measured to obtain fairly consistent homogenization temperatures (Th) to ensure data validity. The T_h of the fluid inclusions measured ranges from 30 ℃ to nearly 250 ℃ with a 90 ℃–190 ℃ modal distribution (Fig. 7). An apparent trend toward higher T_h is observed from the recrystallized dolomicrite to the saddle dolomite and quartz. The T_h of aqueous fluid inclusions in the recrystallized dolomicrite (RH) ranges from 30 ℃ to 50 ℃, with diameters less than 4 μm and vapor–liquid ratios less than 10 %. Most fluid inclusions in the fibrous cements (Cd1) and the isopachous botryoidal dolomites (Cd2) are characterized by irregular ellipse shapes with diameters of approximately 5 μm and vapor–liquid ratios around 15 %, and have T_h ranges of 50 ℃ to 90 ℃. The foliated silty-fine crystalline dolomites (Cd3) usually contains rhombus-shaped fluid inclusions with diameters of approximately 8 μm and vapor–liquid ratios of approximately 30 %. The T_h of fluid inclusions formed in this phase of cement ranges from 90 ℃ to 130 ℃. The diameters of fluid inclusions in the medium-coarse crystalline dolomites (Cd4) are quite large and can reach 18 μm with T_h values ranging from 130 ℃ to 180 ℃. The fluid inclusions in the saddle dolomites (Cd5) and quartz (Q) in Z_2dn^2 have abnormally high T_h ranging between 180 ℃ and 250 ℃, possibly formed under the influence of hydrothermal fluids.

Table 3
Calculated CaO/MgO, FeO/MnO in different microbialites.

Lithology		Cements Ratios				
		Cd1	Cd2	Cd3	Cd4	Cd5
Thrombolitic dolomites	R_1	1.354	1.408	1.444	1.415	1.471
	R_2	0	0.22	0.31	0.30	0.12
Stromatolitic dolomites	R_1	1.442	1.490	0.950	/	1.499
	R_2	0	1.00	0.04	/	0.17
Straticulate dolomites	R_1	1.347	/	1.388	/	1.356
	R_2	1.36	/	1.84	/	3.43

Notes: $R_1 = \frac{w(CaO)}{w(MgO)}$; $R_2 = \frac{w(FeO)}{w(MnO)}$.

5. Discussion

5.1. Diagenesis in microbialitic dolomites

Experienced over 500-million-year geological evolution, the second member of the Dengying Formation (Z_2dn^2) in central Sichuan Basin has undergone multiple alternations due to changing diagenetic environments, resulting in multiple phases of diagenesis and complex pore evolution, including recrystallization, compaction, pressure dissolution, silicification, multiple cementation and dissolution.

Dolomites, including the dolomitized microbialites, are the dominant lithologies in Z_2dn^2. However, the Edicaran period was dominated by an “Aragonite Sea” (Hood et al., 2011) and thus Z_2dn^2 would be prevailed by the deposition of predominant aragonite (Wood et al., 2017). Although geologists are still debating about whether the abundant dolomites in the Dengying Formation were originated from connate deposit (Lei et al., 1992; Wang, 2006) or metasomatism (Liu et al., 2008; Lin, 2015), considering the widespread primary sedimentary fabrics, i.e. acicular texture, we conclude that a reflux infiltration dolomitization model would be a more reasonable scenario (Jin et al., 2019).

Compaction and pressure dissolution are the principal causes of reservoir porosity diminution. However, early dolomitization would enable microbialites to develop rigid frameworks that would resist mechanical compaction. Numerous debris crushed in dolomicrite and

Table 2
Statistics of CaO-MgO contents in different microbialites.

Elements	Lithology								
	Thrombolitic dolomites			Stromatolitic dolomites			Straticulate dolomites		
	Maximum	minimum	average	Maximum	minimum	average	Maximum	minimum	average
CaO	31.21	27.47	29.53	30.61	21.44	28.31	30.62	28.19	29.52
MgO	23.44	20.04	21.08	22.57	17.71	20.49	22.81	20.59	21.53

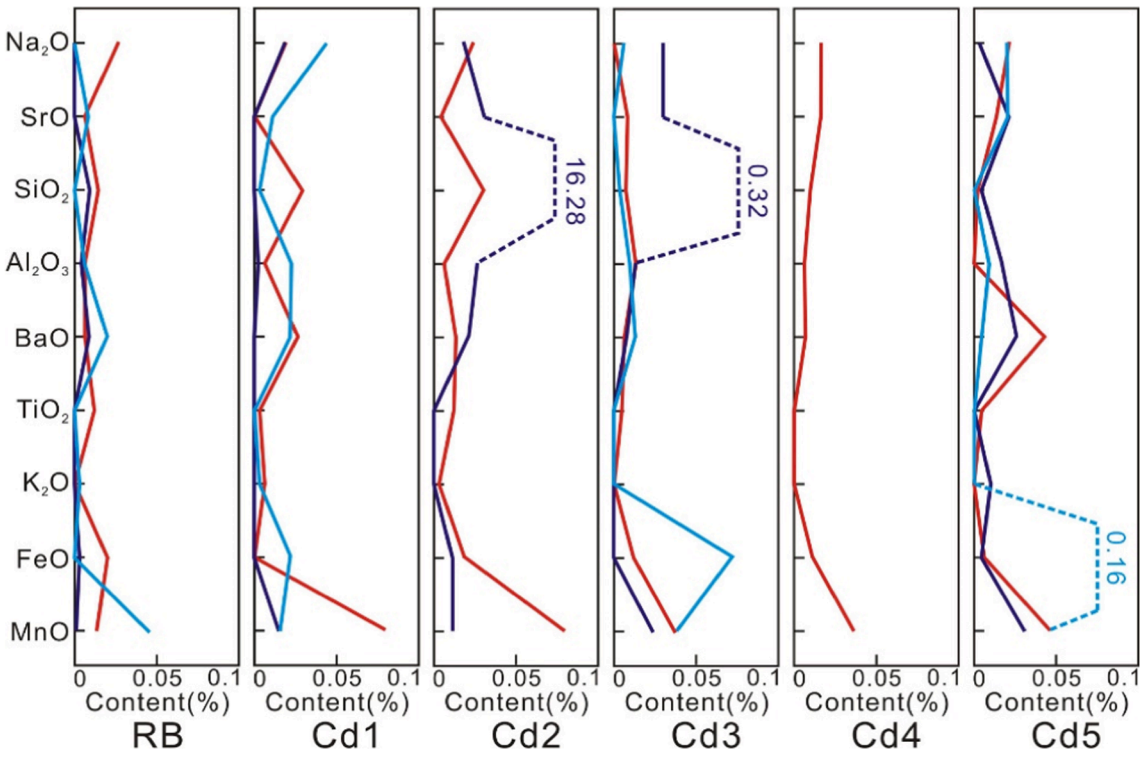

Fig. 5. Major element contents in different microbial dolomites showing variations of major elements in various phases of cement; RH = recrystallized host rock.

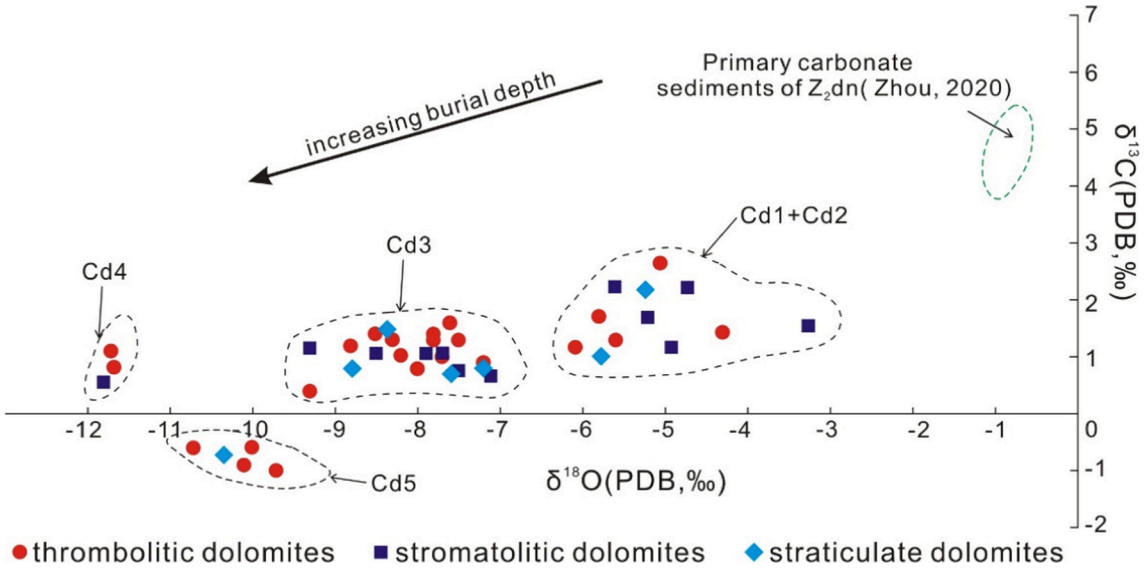

Fig. 6. Cross plot of $\delta^{18}O$ and $\delta^{13}C$ ratios of all dolomite cements in different microbial dolomites showing a progressively decreasing trend in $\delta^{18}O$ and $\delta^{13}C$ ratios with burial depths.

deformation of dolarenite are indicative of the occurrence of strong compaction in Z_2dn^2 (Fig. 8A). The presence of abundant low angle argillaceous stylolites attest the occurrence of pressure dissolution (Fig. 8B).

Cementation is another major cause for reservoir porosity diminution. As mentioned previously, five generations of cement were identified in microbialites based on thin section petrography (Fig. 8C). However, not all microbialites have developed unabridged five generations of cement. For example, Cd4 is completely absent in stromatolitic dolomites, while straticulate dolomites do not contain the Cd2 and Cd4 cements.

Silicification usually develops in stromatolitic dolomites and thrombolitic dolomites. Dark laminar in stromatolite is generally replaced by acicular or columnar quartz with the idiomorphic monocrystal major axis shorter than 0.1 mm, while the light laminar seldom display silicoides. Hence, the primary sedimentary fabrics can be well-preserved. In addition, homogeneous quartz can block the residual pores after the cementation of Cd4 or Cd5 in thrombolitic dolomites (Fig. 8D).

Recrystallization generally occurs in the core of microclots with dark laminar in stromatolite and straticulate dolomite (Fig. 8E). Those parts originally composed of cryptocrystalline microbe deposit or dolomicrite. With increasing burial, temperature and pressure caused dolomicrite to

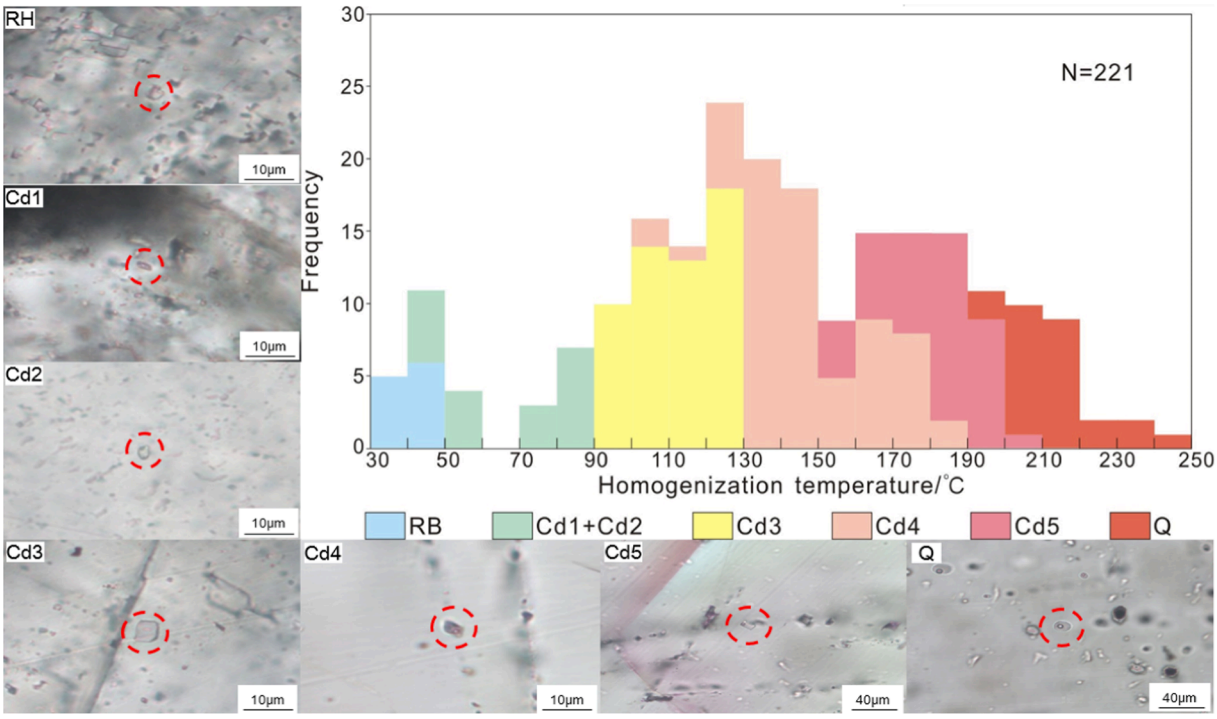

Fig. 7. Histograms of fluid inclusion homogenization temperature (Th) and photomicrographs of typical fluid inclusions in different cements and T_h distribution.

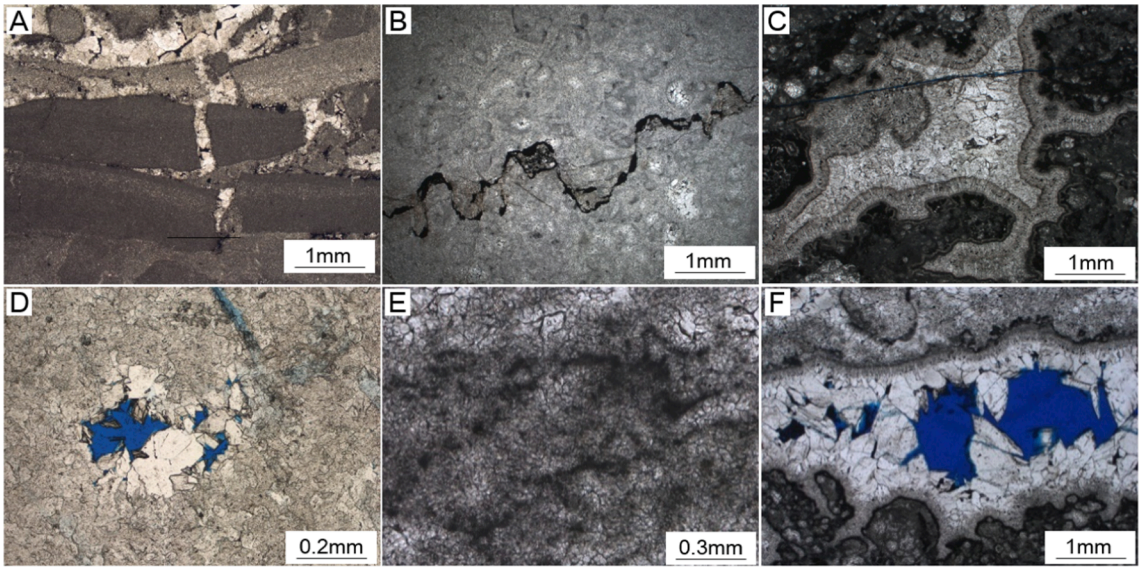

Fig. 8. Photomicrographs showing different diagenetic features of microbialitic dolomites in Z_2dn^2. (A) Compaction-induced fragmentation of dolomicrite debris; (B) Stylolite created by pressure dissolution in recrystallined thromatolitic dolomites; (C) Multiple generations of cementation in thromatolitic dolomites; (D) sub-rhombus quartz, indicative of silicification of subhedral dolomite cements; (E) Recrystalization occurred in endolitic replacement of silty-fine crystalline dolomite from dolomicrite; (F) Abundant secondary pores produced by dissolution in microbialitic dolomites.

recrystallize to microspar or crystal dolomite. The recrystallization intensity shows a negative correlation with the degree of organic enrichments and dissolution remnants.

The Dengying Formation experienced several exposures and superimposed dissolution, with at least three episodes of dissolution. It is well known that microbialites are usually developed in the shallow water areas. Sea-level oscillation would make microbialites exposed frequently, while penecontemporaneous dissolution would create selective interclot pores and framework pores. Two episodes of the Tongwan tectonic movement were recorded over the entire upper Yangtze Platform (Li et al., 2015), which resulted in strong supergene karstification in Z_2dn^2 and Z_2dn^4. Prolonged exposure created plentiful weathered crust, dissolution pores, vugs and caves in Z_2dn^2 (Fig. 8F), accounting for the largest contribution to reservoir quality enhancement (Tang et al., 2013). During the burial stage, hydrocarbon generation and liquid hydrocarbon cracking would generate fluids that are rich in organic acids, carbon dioxide and hydrogen sulfide dissolution, which may dissolve the existing pore networks in microbialites and alters the reservoir petrophysical property.

5.2. Diagenetic sequence and pore evolution models

The essence of diagenetic reaction is the re-equilibration of pore fluids, specifically some rocks would undergo physical or chemical transformation via interaction with pore fluids. According to the variations of diagenetic fluids (Wu et al., 2014; Yuan et al., 2014; Li, 2017), temperature changes (Meng et al., 2011; Liu et al., 2018) and tectonic movement (Xu et al., 2012; Liu et al., 2016), diagenetic evolution of microbial dolomites in Z_2dn^2 can be subdivided into six stages: syndiagenetic, penecontemporaneous, epidiagenetic, eogenetic, mesodiagenetic and telodiagenetic stages (Fig. 9).

The six diagenetic evolution stages can be well correlated to the basin evolution history in the region as reconstructed by Yuan (2008) and Xu (2017) (Fig. 9). After the deposition of the Dengying Formation, with an extensive marine transgression in the Early Cambrian, thick mudstone and shale deposition not only filled the aulacogen but also capped on subaqueous paleo-uplift in the Sichuan Basin (Li et al., 2014). The late Caledonian orogeny (Late Silurian to Early Devonian) caused the entire upper Yangtze Plate uplifted, which resulted in massive stratigraphic erosion until the Permian (Wang, 2006). Following the equilibrated subsidence persist from Permian to middle Triassic, the upper Yangtze Platform experienced rapidly deposition and reached the largest burial depth (over 7000 m) in the Cretaceous (Mei et al., 2014). Subsequent heterogeneous uplift occurred in the late Yanshanian (Cretaceous) and the Himalayan (Eocene to Quaternary) orogenies (Fig. 9).

5.2.1. Syndiagenetic stage

The Upper Yangtze plate located in 30 °N (northern latitude) in the Ediacaran (Christopher, 2009), with sea-water temperatures varying from 20 ℃ to 25 ℃ (Meng et al., 2011). A largely restricted carbonate platform sedimentary environment dominated the central Sichuan Basin during Z_2dn^2 (Hu et al., 2019). Impeded seawater circulation and high temperatures resulted in strong evaporation. Concentrated brines continuously infiltrated into the lower strata and disequilibrated the stationary water–rock system, causing the deposition of $CaCO_3$ and $CaSO_4$. Evaporation thus promoted an increase of the ratio of $c(Mg^{2+})$ over $c(Ca^{2+})$ and promoted dolomitization. In addition, microbial metabolisms can reduce the kinetic barrier of dolomitization by dehydrate Mg^{2+} from $CaSO_4$ (Burns et al., 2000), increasing the availability of Mg^{2+} (Lith et al., 2003) or increasing the fluid alkalinity (Sánchez-Román et al., 2009). However, the dolomitization rates are heterogeneous among different petrofabrics. Microbial clots and dark laminae rich in cyanobacteria would be dolomitized earlier than the interclots in thromatolites and light laminae in stromatolites.

Microbialites deposited in paleotopographic highs would have experienced frequent exposures. Aragonite sediments are more soluble in meteoric environment and may create primary framework pores with high porosity in stromatolitic dolomites and thromatolitic dolomites. The porosity may reach 40 % in the modern Great Salt Lake analogue (Thomas et al., 2015). Although the majority of contemporaneous selective dissolution pores would be sealed during subsequent diagenesis, they can enlarge the superficial area and enhance the rate of physical and chemical reaction between microbialites and the formation water.

5.2.2. Penecontemporaneous stage

When microbialites become submerged, brine would re-enter the framework pores in thromatolitic dolomites and stromatolitic dolomites,

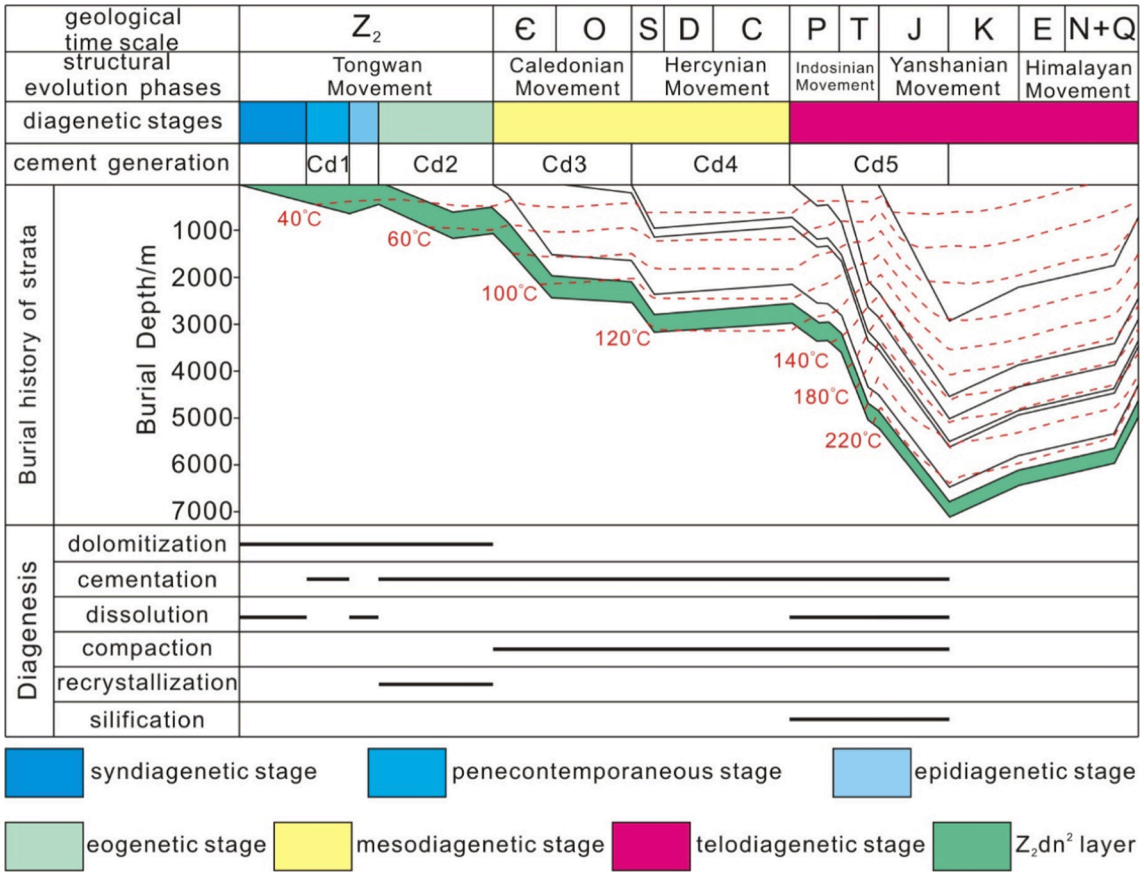

Fig. 9. Diagenetic sequence of microbial-dominated dolomites in Z_2dn^2, correlated with the burial and thermal history model of Well GS-1 in the study area from Xu (2017). Geohistory and thermal history reconstruction is based on apatite fission track analysis from core samples from MX24 Well and MX58 Well (see Fig. 1 for well locations) with up to 2000 m strata being eroded away (Yuan, 2008). The basin model was calibrated with vitrinite reflectance and present day bore hole temperature data.

and as well as the bird's-eye pores in straticulate dolomites. With increasing burial and temperature, fascicular and fibrous cements (Cd1) would be developed along the periphery of the primary pores due to elevated pressure and temperature. The fascicular acicular dolomite would become dominated in the birds'-eyes pores while fibrous cements would develop in stromatolitic dolomites. Similar elemental distribution pattern of the host rock and Cd1 imply that the formation water would be still connected with sea water. More negative $\delta^{13}C$ and $\delta^{18}O$ values (1 ‰ to 2.6 ‰ and −6.1 ‰ to −3.2 ‰, respectively) and higher T_h (40 ℃–60 ℃) of Cd1 compared with the host rock suggest that Cd1 was generated after the syndiagenetic stage. Widespread fascicular Cd1 growth around the primary framework pores is indicative of high permeability and an open circulation system. Replenished sea water would provide adequate Mg^{2+} for dolomitization. However, the reduction of $c(Mg^{2+})/c(Ca^{2+})$ and the weakening of microbial metabolism would mitigate the dolomitization rate, which allows fibrous cements to be mimetically replaced by dolomites.

5.2.3. Epidiagenetic stage

The Tongwan movement (Episode I) caused uplift of the entire Yangtze plate and resulted in the eluviation of the top of Z_2dn^2 by meteoric water (Li et al., 2015; Zhu et al., 2019). De-dolomitized aragonite and high-Mg calcite petrofabrics in the thrombolite clots (i.e. endolithic debris within clots) and light laminae of stromatolites were preferentially dissolved, creating enlarged framework pores, interclot pores, intraclot pores, vugs, stratiform dissolution pores and minor moldic pores. Nearly all aragonites can be dissolved or transformed into magnesium calcites in approximately 0.6 Myr (Huang et al., 2020). Dolomitized endolithic clots were developed in thromatolites and the dark laminae in stromatolites or straticulates. However, secondary pores created by meteoric water dissolution were less well developed in straticulates compared with stromatolites and thrombolites due to their poor interconnectivity.

5.2.4. Eogenetic stage

Accompanied by extensive transgression (Zhou et al., 2017), Z_2dn^2 was rapidly buried to the hyporheic zone. Multiple isopachous layers (Cd2) started to cement around enlarged framework pores, interclot pores, stratiform dissolution pores and vugs owing to oscillating shallow burial depths, still preserving high porosity and good connectivity in stromatolites and thromatolites. Cd2 is rarely generated in intraclot dissolution pores and moldic pores due to their lower porosity and poor connectivity. The relatively low ω(SrO), ω(Na_2O) and ω(K_2O) of Cd2 indicate that cementation was still influenced by meteoric water. The comparable $\delta^{13}C$ and $\delta^{18}O$ ratios of Cd2 and Cd1, and as well as the relatively low fluid inclusion T_h (50 ℃–90 ℃) further attest a shallow burial setting. The gradual increase of the formation temperature dissolved more Mg^{2+} and reduced the dolomitization activation energy, resulting in the transformation of abundant magnesium-rich calcites into dolomites within 5.4 Myrs (Shen et al., 2021).

5.2.5. Mesodiagenetic stage

With increasing burial, elevated temperature and pressure triggered compaction and cementation again. Foliated silty-fine crystalline dolomite cements (Cd3) overgrew on isopachous cements (Cd2), followed by medium-coarse crystalline dolomite cements (Cd4). In the mesodiagenetic stage, the majority of the intraclot pores and moldic pores had been filled, while most vugs, large framework pores and interclot pores in stromatolitic dolomites and thromatolitic dolomites were reduced dramatically. The mottled dull-red luminescence, xenomorphic to subhedral crystal morphology along with characteristic $\delta^{13}C$ (0.4 ‰–1.6 ‰, avg. 1.1 ‰) and $\delta^{18}O$ (−9.3 ‰ to −7.1 ‰, avg. −8.1 ‰) ratios of Cd3 indicate that they may have been directly precipitated from the interstitial water. The majority of secondary pores in straticulate dolomites are fully occupied by the Cd3 cement. The fluid inclusion T_h of Cd3 ranges from 90℃ to 130℃, corresponding to burial depths of 2.0 km to 3.5 km on the burial history diagram.

The clean and transparent Cd4 cement is usually observed in residual space of vugs, interclot pores and framework pores in thromatolitic dolomites, but are seldom seen in the stratiform dissolution pores in stromatolitic dolomites. Idiomorphic monocrystal, yellow luminescence, relative high ω(MnO), ω(FeO) and lighter $\delta^{18}O$ suggested that Cd4 may have formed in a stable and enclosed system under a relatively high temperature. This is consistent with high fluid inclusion T_h values of Cd4, ranging from 130 ℃ to 150 ℃. Oil generated in the Qingzhusi Formation migrated into Z_2dn^2 in two episodes: during the Late Silurian to the Devonian (Yuan et al., 2014), and during the Late Permian to the Triassic (Ni et al., 2018). The presence of hydrocarbon inclusions in Cd4 confirms the existence of a secondary episode of oil migration.

5.2.6. Telodiagenetic stage

Rb-Sr dating of sphalerite in Z_2dn^2 indicates that hydrothermal fluids upwelling along major (deep) faults in the Late Permian (Jiang et al., 2016), which triggered widespread silicification and thermochemical sulfate reduction (TSR). Non-selective silicification occurred near faults while selective silicification occurred away from faults because hydrothermal fluid migrated preferably along interconnecting pores, especially along stratiform dissolution pores. The fluid inclusion T_h value in the quartz cement reaches 250 ℃, significantly higher than the maximum burial temperature (ca. 230 ℃; Hu et al., 2020). Major and trace elements such as ω(FeO), ω(MnO) and ω(SrO) were also enriched dramatically in the quartz.

The bright yellow cathode luminescence of saddle dolomites in Cd5, with the most negative $\delta^{18}O$ and $\delta^{13}C$ ratios, indicates that Cd5 was directly precipitated during the telogidagenetic stage. The fluid inclusion T_h values of saddle dolomites range from 160 ℃ to 210 ℃, corresponding to burial depths of 4.5 km to 7.0 km. The abnormal negative $\delta^{13}C$ values in the dolomite may result from CO_2 generated by oil cracking or TSR (Liu et al., 2016). Organic acids and CO_2 derived from oil cracking and TSR may have enhanced the fluid acidities and consequently dissolved the periphery of the saddle dolomites (Zhu et al., 2006). However, the deep burial dissolution mechanisms and spatial distribution ranges will need to be further investigated.

The absence of bitumen in fractures developed during the Yanshannian and Himalayan orogenies suggested that oil cracking occurred much earlier, probably before the Jurassic (Wang et al., 2014). Although fractures cannot create much reservoir accommodation space, it can significantly improve reservoir quality by interconnecting residual pores.

5.3. Implications for exploring microbialite reservoir plays

The crucial factors for developing high-quality microbialite reservoirs in Z_2dn^2 including high-energy sedimentary environments, early dolomitization and supergene karst. Modern analogues reveal that thrombolites and stromatolites are preferably developing in high-energy environments. The accumulative thickness of microbially-dominated reservoirs can exceed 200 m in the platform margin while reach no more than 80 m in the inner platform in Z_2dn^2. Continuous seawater circulation provides essential materials for rapid microbial growth and create framework pores in microbialites. The entire platform was uplifted by the Tongwan I tectonic movement immediately after its deposition and supergene karsting enlarged the well-developed interconnected but weakly-cemented pores. The lower concentrations of Na, Sr and K in Cd1 and Cd2 in dissolution vugs compared with that in recrystallized host rock (RH) suggest that supergene karsting may have occurred in an open system. Unsaturated meteoric water and persistent dissolution could generate abundant dissolution vugs with diameters of 1–6 cm in cores. Early dolomitization, occurred from the syndiagenetic stage to the eogenetic stage, developed rigid rock frameworks which can resist subsequent compaction and pressure dissolution. Although superimposed cementation and silicification reduced porosity largely,

abundant residual pores have been preserved in the high-quality microbialite reservoirs in Z_2dn^2. In summary, highly interconnected primary pores in microbialites reservoirs were generated under high-energy sedimentary environment and were further enlarged by early supergene dissolution, while early dolomitization created rigid rock frameworks which have contributed to the preservation of high-quality reservoirs.

6. Conclusions

We have documented the complex diagenetic history and pore evolution of different microbial-dominated dolomites in Z_2dn^2 in central Sichuan Basin by using a variety of data and methods. Five generations of cement are identified in microbialitic dolomites based on element distribution patterns, carbon and oxygen isotope characteristics, as well as fluid inclusion homogenization temperatures. During the syndiagenetic stage, early dolomitization converted aragonite while preserved their primary petrofabrics, while frequent exposures resulted in the syngenetic dissolution. When submerged, fascicular and fibrous cements (Cd1) would be developed along the periphery of the primary pores during the penecontemporaneous stage. The Tongwan I movement resulted in the eluviation of Z_2dn^2, which created abundant enlarged framework pores, interclot pores, vugs, stratiform dissolution pores and minor moldic pores in microbialites. Although compaction, cementation (Cd2-Cd5) and silification lasted from the eogenetic to the telodiagenetic stage which immensely reduced the porosity, the development of residual dissolution pores is primarily responsible for the formation of the high-quality Edicaran microbial-dominated dolomite reservoirs in Z_2dn^2 in the central Sichuan Basin.

Declaration of Competing Interest

The authors declare that they have no known competing financial interests or personal relationships that could have appeared to influence the work reported in this paper.

Data availability

Data will be made available on request.

Acknowledgements

This research is financially supported by the Strategic Priority Research Program of the Chinese Academy of Sciences (Grant No: XDA14010401), and the National Natural Science Foundation of China Grants (No: 42002115, No: 41821002). We are also grateful to the editors and two anonymous reviewers for their constructive comments and suggestions.

Appendix 1. Information of 126 samples collected from 10 wells

MX8 Well		
Sample Number	Sample Depth(m)	Lithology
mx8-Z2dn2-1	5425.1	straticulate dolomite
mx8-Z2dn2-2	5425.43	fine crystalline dolomite
mx8-Z2dn2-3	5425.64	thrombolitic dolomite
mx8-Z2dn2-4	5426	fine crystalline dolomite
mx8-Z2dn2-5	5353.1	silty crystalline dolomite
mx8-Z2dn2-6	5355	silty crystalline dolomite
mx8-Z2dn2-7	5359	straticulate dolomite
mx8-Z2dn2-8	5361	stromatolitic dolomite
mx8-Z2dn2-9	5362.33	fine crystalline dolomite
mx8-Z2dn2-10	5363.5	thrombolitic dolomite
MX9 Well		
Sample Number	Sample Depth(m)	Lithology
mx9-Z2dn2-1	5432	thrombolitic dolomite
mx9-Z2dn2-2	5435	fine crystalline dolomite
mx9-Z2dn2-3	5447	stromatolitic dolomite
mx9-Z2dn2-4	5448	thrombolitic dolomite
mx9-Z2dn2-5	5450	thrombolitic dolomite
mx9-Z2dn2-6	5451	stromatolitic dolomite
mx9-Z2dn2-7	5495	thrombolitic dolomite
mx9-Z2dn2-8	5501	thrombolitic dolomite
mx9-Z2dn2-9	5502	thrombolitic dolomite
mx9-Z2dn2-10	5513	fine crystalline dolomite
mx9-Z2dn2-11	5522	thrombolitic dolomite
MX10 Well		
Sample Number	Sample Depth(m)	Lithology
mx10-Z2dn2-1	5486.04	thrombolitic dolomite
mx10-Z2dn2-2	5484.64	thrombolitic dolomite
mx10-Z2dn2-3	5482.25	dolarenite
mx10-Z2dn2-4	5481.52	dolarenite
mx10-Z2dn2-5	5481.25	dolarenite
mx10-Z2dn2-6	5481.1	fine crystalline dolomite
mx10-Z2dn2-7	5479.7	dolarenite
mx10-Z2dn2-8	5477.5	dolarenite
mx10-Z2dn2-9	5477.6	dolarenite
mx10-Z2dn2-10	5477.4	dolarenite
mx10-Z2dn2-11	5476.74	straticulate dolomite
mx10-Z2dn2-12	5476.1	straticulate dolomite
mx10-Z2dn2-13	5475.81	straticulate dolomite
MX11 Well		
Sample Number	Sample Depth(m)	Lithology
mx11-Z2dn4-1	5151.33	straticulate dolomite
mx11-Z2dn2-1	5495.98	straticulate dolomite
zt1-Z2dn2-27	4937.5	straticulate dolomite
zt1-Z2dn2-28	4935.1	straticulate dolomite
GS1 Well		
Sample Number	Sample Depth(m)	Lithology
gs1-Z2dn2-1	5318	thrombolitic dolomite
gs1-Z2dn2-2	5319	straticulate dolomite
gs1-Z2dn2-3	5320	thrombolitic dolomite
gs1-Z2dn2-4	5322	fine crystalline dolomite
gs1-Z2dn2-5	5323	silty crystalline dolomite
gs1-Z2dn2-6	5324	thrombolitic dolomite
gs1-Z2dn2-7	5325	straticulate dolomite
gs1-Z2dn2-8	5326	stromatolitic dolomite
gs1-Z2dn2-9	5327	thrombolitic dolomite
gs1-Z2dn2-10	5379	fine crystalline dolomite
gs1-Z2dn2-11	5380	thrombolitic dolomite
gs1-Z2dn2-12	5381	thrombolitic dolomite
GS6 Well		
Sample Number	Sample Depth(m)	Lithology
gs6-Z2dn2-1	5485.33	fine crystalline dolomite
gs6-Z2dn2-2	5382.41	straticulate dolomite
gs6-Z2dn2-3	5381.23	dolomicrite
gs6-Z2dn2-4	5379.4	silty crystalline dolomite
gs6-Z2dn2-5	5377.62	thrombolitic dolomite
gs6-Z2dn2-6	5372.92	thrombolitic dolomite
gs6-Z2dn2-7	5372.5	fine crystalline dolomite
gs6-Z2dn2-8	5372.35	fine crystalline dolomite
gs6-Z2dn2-9	5371.74	dolarenite
gs6-Z2dn2-10	5368.28	silty crystalline dolomite
gs6-Z2dn2-11	5366.41	silty crystalline dolomite
gs6-Z2dn2-12	5364.13	silty crystalline dolomite
gs6-Z2dn2-13	5361.27	dolomicrite
gs6-Z2dn2-14	5360.16	fine crystalline dolomite
gs6-Z2dn2-15	5359.73	fine crystalline dolomite
gs6-Z2dn2-16	5037.43	straticulate dolomite
gs6-Z2dn2-17	5035.4	fine crystalline dolomite
GS11 Well		
Sample Number	Sample Depth(m)	Lithology
gs11-Z2dn2-1	5380.9	thrombolitic dolomite
gs11-Z2dn2-2	5378.71	straticulate dolomite
gs11-Z2dn2-3	5378.1	straticulate dolomite
gs11-Z2dn2-4	5376.97	straticulate dolomite
gs11-Z2dn2-5	5376.45	straticulate dolomite
gs11-Z2dn2-6	5375.95	stromatolitic dolomite
gs11-Z2dn2-7	5375.52	straticulate dolomite

(*continued on next page*)

(*continued*)

mx11-Z2dn2-2	5494.64	dolarenite	gs11-Z2dn2-8	5373.6	silty crystalline dolomite
mx11-Z2dn2-3	5494.02	fine crystalline dolomite	gs11-Z2dn2-10	5372.5	straticulate dolomite
mx11-Z2dn2-4	5492.49	thrombolitic dolomite	gs11-Z2dn2-11	5371.74	straticulate dolomite
mx11-Z2dn2-5	5490.82	dolarenite	gs11-Z2dn2-12	5369.9	silty crystalline dolomite
mx11-Z2dn2-6	5488.82	fine crystalline dolomite	gs11-Z2dn2-13	5368.23	dolomicrite
mx11-Z2dn2-7	5486.37	thrombolitic dolomite	gs11-Z2dn2-14	5366.1	dolarenite
mx11-Z2dn2-8	5485.17	fine crystalline dolomite	gs11-Z2dn2-15	5365.17	straticulate dolomite
mx11-Z2dn2-9	5484.32	silty crystalline dolomite	Z4 Well		
mx11-Z2dn2-10	5482.25	straticulate dolomite	Sample Number	Sample Depth(m)	Lithology
ZT1 Well			z4-Z2dn2-1	4497	thrombolitic dolomite
Sample Number	Sample Depth(m)	Lithology	z4-Z2dn2-2	4533	straticulate dolomite
zt1-Z2dn2-1	4979.1	fine crystalline dolomite	z4-Z2dn2-3	4554	straticulate dolomite
zt1-Z2dn2-2	4977.3	thrombolitic dolomite	z4-Z2dn2-4	4562	straticulate dolomite
zt1-Z2dn2-4	4974.3	fine crystalline dolomite	W117 Well		
zt1-Z2dn2-5	4971.7	thrombolitic dolomite	Sample Number	Sample Depth(m)	Lithology
zt1-Z2dn2-7	4969.4	fine crystalline dolomite	w117-Z2dn2-1	3024	fine crystalline dolomite
zt1-Z2dn2-9	4966.2	fine crystalline dolomite	w117-Z2dn2-2	3026	fine crystalline dolomite
zt1-Z2dn2-10	4963.8	fine crystalline dolomite	w117-Z2dn2-3	3039	silty crystalline dolomite
zt1-Z2dn2-12	4962.4	silty crystalline dolomite	w117-Z2dn2-4	3045	thrombolitic dolomite
zt1-Z2dn2-13	4961	straticulate dolomite	w117-Z2dn2-5	3102	thrombolitic dolomite
zt1-Z2dn2-14	4959.6	fine crystalline dolomite	w117-Z2dn2-6	3103	thrombolitic dolomite
zt1-Z2dn2-15	4958.9	dolarenite	w117-Z2dn2-7	3107	thrombolitic dolomite
zt1-Z2dn2-16	4955.6	fine crystalline dolomite	w117-Z2dn2-8	3123	stromatolitic dolomite
zt1-Z2dn2-17	4954.2	dolarenite	w117-Z2dn2-9	3129	straticulate dolomite
zt1-Z2dn2-18	4952.1	silty crystalline dolomite	w117-Z2dn2-10	3131	silty crystalline dolomite
zt1-Z2dn2-19	4950.3	silty crystalline dolomite	w117-Z2dn2-11	3136	thrombolitic dolomite
zt1-Z2dn2-24	4940.5	straticulate dolomite	w117-Z2dn2-12	3158	thrombolitic dolomite
zt1-Z2dn2-25	4939.9	thrombolitic dolomite	w117-Z2dn2-13	3160	thrombolitic dolomite
zt1-Z2dn2-26	4939	dolarenite	w117-Z2dn2-14	3161	thrombolitic dolomite

Appendix 2. Major elements contents of carbonate cements presented in Fig. 5

Lithology	Fabric	Na_2O	SrO	SiO_2	Al_2O_3	MgO	SO_3	CaO	BaO	TiO_2	K_2O	FeO	MnO	Total
Thrombolitic dolomites	Host Rock	0.05	##	0.05	0.01	21.85	0.15	29.24	##	##	0.01	0.04	0.03	51.42
	Host Rock	0.05	0.01	##	0.02	21.05	0.07	28.40	##	##	##	0.02	0.01	49.63
	Host Rock	0.04	0.01	0.03	0.02	21.74	0.01	30.11	0.01	0.01	0.01	0.01	0.01	52.01
	Host Rock	0.05	##	0.04	##	23.44	##	30.89	##	##	0.01	0.04	0.02	54.49
	Host Rock	0.02	##	0.02	##	20.72	0.05	28.73	##	##	##	0.03	0.02	49.59
	RH	0.04	0.01	0.03	##	22.86	##	30.13	0.02	##	##	0.02	0.02	53.13
	RH	0.04	##	##	0.02	21.91	0.02	29.15	##	0.04	##	0.02	0.01	51.21
	RH	##	##	0.01	##	21.18	##	29.65	##	##	##	0.02	0.01	50.86
	Cd1	0.02	##	0.03	0.01	20.37	##	27.59	0.03	##	0.01	##	0.08	48.13
	Cd2	0.03	0.02	0.03	0.01	20.72	##	28.37	##	##	##	0.02	0.02	49.22
	Cd2	0.04	##	0.06	##	20.45	0.02	28.35	0.02	##	0.01	0.03	0.03	49.00
	Cd2	##	##	##	0.01	21.30	##	31.21	##	0.04	##	0.02	0.19	52.76
	Cd3	##	##	0.03	0.02	20.96	##	29.95	##	##	##	0.03	##	50.99
	Cd3	##	##	##	##	20.64	##	29.52	0.02	##	##	0.01	0.01	50.20
	Cd3	##	0.02	##	0.02	20.97	0.01	30.51	##	##	##	0.01	##	51.55
	Cd3	##	0.02	0.01	0.01	20.32	##	29.76	0.01	##	##	0.01	0.02	50.16
	Cd3	##	##	##	##	20.04	0.04	29.48	0.01	0.02	##	0.01	0.02	49.62
	Cd3	##	##	##	0.02	20.63	0.04	29.26	##	##	##	##	0.16	50.12
	Cd4	0.02	##	0.01	##	20.47	0.01	27.47	##	##	##	0.02	0.03	48.02
	Cd4	0.01	0.03	0.01	0.01	20.78	##	30.92	0.01	##	##	##	0.04	51.83
	Cd5	0.01	0.03	0.01	##	20.60	0.02	30.35	0.05	##	##	##	0.01	51.08
	Cd5	0.03	##	##	##	20.86	##	30.67	0.04	0.01	##	0.01	0.08	51.70
Stromatolitic dolomites	Host Rock	##	##	##	0.03	20.32	0.01	29.51	##	##	0.01	0.01	0.01	49.90
	Host Rock	##	##	0.04	##	21.25	0.01	30.59	##	##	##	0.05	0.01	51.95
	RH	##	##	0.01	0.01	21.01	0.01	30.61	0.01	##	##	##	##	51.65
	Cd1	0.02	##	##	##	20.81	0.01	30.02	##	##	##	##	0.01	50.87
	Cd2	0.02	0.03	16.28	0.03	17.71	0.04	26.37	0.02	##	##	0.01	0.01	60.52
	Cd3	0.03	0.03	0.32	0.01	22.57	0.03	21.44	0.01	##	##	##	0.02	44.46
	Cd5	##	0.02	0.01	0.02	19.80	0.02	29.67	0.03	##	0.01	0.01	0.03	49.61
	Q	0.01	0.29	99.88	0.06	##	##	0.04	0.02	0.04	##	0.01	##	100.35
	Q	0.03	0.31	97.32	##	##	##	0.01	##	##	##	##	##	97.67
Straticulate dolomites	Host Rock	0.01	##	##	##	21.95	0.03	29.06	##	##	##	0.04	0.02	51.11
	Host Rock	0.01	0.01	##	##	21.77	0.03	29.03	0.04	0.01	##	0.02	0.01	50.94
	RH	##	0.02	##	##	20.95	##	29.52	0.04	##	##	##	0.05	50.57
	RH	##	##	##	0.01	21.25	0.02	28.75	##	##	##	##	0.04	50.06
	Cd1	0.05	0.03	##	0.02	21.64	0.02	30.62	0.02	##	##	0.01	0.02	52.42
	Cd1	0.03	##	0.01	0.03	22.81	##	29.73	0.04	##	##	0.03	0.01	52.70
	Cd1	0.05	##	##	0.02	21.93	0.02	29.07	##	##	0.01	0.02	0.02	51.14
	Cd3	##	##	0.01	##	21.28	0.01	29.62	0.02	##	##	0.02	0.02	50.97

(*continued on next page*)

(*continued*)

Lithology	Fabric	Na_2O	SrO	SiO_2	Al_2O_3	MgO	SO_3	CaO	BaO	TiO_2	K_2O	FeO	MnO	Total
	Cd3	##	##	##	##	21.77	##	28.19	##	##	##	0.04	0.04	50.04
	Cd3	##	0.01	0.01	0.01	21.18	##	29.79	##	##	##	0.04	0.03	51.08
	Cd3	0.01	##	##	0.01	20.59	0.02	29.65	0.05	##	0.01	0.25	0.06	50.66
	Cd3	0.01	##	##	0.02	21.43	##	30.17	##	##	##	##	0.04	51.66
	Cd5	0.02	0.03	##	0.02	22.15	0.04	29.29	0.01	##	##	0.02	##	51.57
	Cd5	0.02	0.01	##	##	21.41	0.01	29.78	##	##	##	0.30	0.09	51.61

RH: recrystallized host rock; Q: quartz; ##: undetected;

References

Ana, C.A., Luís, V.D., Alexandre, P.S., 2021. The challenging carbonates from the Pre-Salt reservoirs offshore Brazil: facies, palaeoenvironment and diagenesis. J. S. Am. Earth Sci. 108, 1–23.

Bruno, E.M.L., Luiz, F.D.R., 2019. Deposition, diagenetic and hydrothermal processes in the Aptian Pre-Salt lacustrine carbonate reservoirs of the northern Campos Basin, offshore Brazil. Sed. Geol. 383, 55–81.

Burns, S.J., McKenzie, J.A., Vasconcelos, C., 2000. Dolomite formation and biogeochemical cycles in the Phanerozoic. Sedimentology 47, 49–61.

Christopher R.S., 2009. Late Proterozoic plate tectonics and palaeogeography: A tale of two supercontinents, Rodinia and Pannotia. Geological Society 326, 67-83.

Deng, B., Guan, P., Pang, L., Liu, P.X., Jin, Y.Q., Zhang, Y.Q., 2018. Genesis of Excellent Xiaoerbulak Microbial Carbonate Reservoir in Kalpin Area of Tarim Basin. NW China. Acta Sedimentologica Sinica 36 (6), 1218–1332.

Du, J.H., Wang, Z.C., Zou, C.N., Xu, C.C., Shen, P., Zhang, B.M., Jiang, H., Huang, S.P., 2016. Discovery of intra-cratonic rift in the Upper Yangtze and its control effect on the formation of Anyue giant field. Acta Pet. Sin. 37 (1), 1–16.

Duan, J.B., Jin, M.D., Fan, Z.W., Zhu, X., Liu, Y.T., 2021. Characteristics and favorable plays for high-quality reservoirs in the Middle Triassic Lei 4 Member, Yuanba area, northeastern Sichuan Basin. Oil Gas Geol. 42 (4), 898–908.

Fei, B.S., Wang, J.H., 2005. Cases of Discovery and Exploration of Marine Fields in China (Part 3): Renqiu Buried-hill Oilfield, Bohaiwan Basin. Marine Origin Petroleum Geology 10 (3), 43–50.

Frantz, C.M., Victoria, A.P., Marenco, P.J., Tripati, A., Berelson, W.M., Corsetti, F.A., 2014. Dramatic local environmental change during the Early Eocene Climatic Optimum detected using high resolution chemical analyses of Green River Formation stromatolites. Palaeogeogr. Palaeoclimatol. Palaeoecol. 405, 1–15.

Grotzinger, J., Rawahi, Z.A., 2014. Depositional facies and platform architecture of microbialite-dominated carbonate reservoirs, Ediacaran-Cambrian Ara Group, Sultanate of Oman. AAPG Bull.. 98 (8), 1453–1494.

Haddad, S.A., Mancini, E.A., 2013. Reservoir characterization, modeling, and evaluation of Upper Jurassic Smackover microbial carbonate and associated facies in Little Cedar Creek field, southwest Alabama, eastern Gulf coastal plain of the United States. AAPG Bull. 97 (11), 2059–2083.

Hood, A.S., Wallace, M.W., Drysdale, R.N., 2011. Neoproterozoic aragonite-dolomite seas? Widespread marine dolomite precipitation in Cryogenian reef complexes. Geology 39, 871–874.

Hu, Y.J., Cai, C.F., Chelsea, L.P., Liu, D.W., Lei, J., He, X.Y., Shi, S.F., Adrian, I., 2020. Dolomitization history and porosity evolution of a giant, deeply buried Ediacaran gas field (Sichuan Basin, China). Precambr. Res. 338, 1–21.

Hu, M.Y., Gao, D., Wei, G.Q., Yang, W., Xie, W.R., 2019b. Sequence stratigraphy and facies architecture of a moundshoal-dominated dolomite reservoir in the late Ediacaran Dengying Formation, central Sichuan Basin, SW China. Geol. J. 54, 1653–1671.

Hu, A., Shen, A., Wang, Y., Pan, L., Wang, Y., Hao, Y.i., Zhang, J., 2019a. The geochemical characteristics and origin analysis of the botryoidal dolomite in the Upper Sinian Dengying Formation in the Sichuan Basin, China. J. Natl. Geosci. 4 (2), 93–100.

Hu, A.P., Shen, A.J., Zheng, J.F., Wang, X., Wang, X.F., 2021. The classification, facies and sedimentary models of microbialites. Marine Origin Petroleum Geology 26 (1), 1–15.

Huang, T.Y., Chen, D.Z., Ding, Y., Zhou, X.Q., Zhang, G.J., 2020. SIMS U-Pb Zircon Geochronological and Carbon Isotope Chemostratigraphic Constraints on the Ediacaran-Cambrian Boundary Succession in the Three Gorges Area, South China. J. Earth Sci. 31 (1), 69–78.

Jiang, Y.Q., Tao, Y.Z., Gu, Y.F., Wang, Y.B., Qiang, Z.T., Jiang, N., Lin, G., Jiang, C., 2016. Hydrothermal dolomitization in Sinian Dengying Formation, Gaoshiti-Moxi area, Sichuan Basin, SW China. Pet. Explor. Dev. 43 (1), 51–60.

Jin, M.D., Tan, X.C., Li, B.S., Zhu, X., Zeng, W., Lian, C.B., 2019. Genesis of Dolomite in the Sinian Dengying Formation in the Sichuan Basin. Acta Sedimentol. Sin. 37 (3), 443–454.

Kenter, J.A.M., Harris, P.M., Porta, G.D., 2005. Steep microbial boundstone-dominated platform margins: examples and implications. Sed. Geol. 178, 5–30.

Lan, C.J., Xu, Z.H., Ma, X.L., Hu, C., Chen, H.R., Zou, H.Y., 2019. Development and distribution of mound-shoal complex in the Sinian Dengying Formation, Sichuan Basin and its control on reservoirs. Acta Pet. Sin. 40 (9), 1069–1084.

Lei, H.Y., Zhu, L.F., 1992. Study of origin of the Sinian algal and nonalgal dolomitites in Sichuan Basin. Acta Sedimentol. Sin. 10 (2), 69–78.

Li, S.J., Gao, P., Huang, B.Y., Wang, H.J., Wo, Y.J., 2018. Sedimentary constraints on the tectonic evolution of Mianyang-Changning trough in the Sichuan Basin. Oil Gas Geol. 39 (5), 889–898.

Li, W., Liu, J.J., Deng, S.W., Zhang, B.M., Zhou, H., 2015. The nature and role of Late Sinian-Early Cambrian tectonic movement in Sichuan Basin and its adjacent areas. Acta Pet. Sin. 36 (5), 546–563.

Li, L., Tan, X.C., Zeng, W., Zhou, T., Yang, Y., Hong, H.T., Luo, B., Bian, L.Z., 2013. Development and reservoir significance of mud mounds in Sinian Dengying Formation, Sichuan Basin. Pet. Explor. Dev. 40 (6), 666–673.

Li, W., Yi, H.Y., Hu, W.S., Yang, G., Xiong, X., 2014a. Tectonic evolution of Caledonian paleohigh in the Sichuan Basin and its relationship with hydrocarbon accumulation. Nat. Gas Ind. 34 (3), 8–15.

Li, Y.N., Zheng, R.C., Pang, Y.C., Sun, H.Q., 2014b. Lithology Characteristic and Sedimentary Environment of the Member 3 of Dengying Formation, in Yangba Area, Northeast Sichuan. Sci. Technol. Eng. 14 (5), 204–210.

Li, X.Y., 2009. The fine study of Sequence Stratigraphy and Reservoir of The Sinian System Dengying formation in the south-east of Sichuan, Master's thesis, Chengdu University of Technology, Chengdu, 37p. (in Chinese with English abstract).

Li, W.P., 2017. Geochemistry of sedimentary carbonates from the late Ediacaran to the early Cambrian in the lower Yangtze region of South China. Doctor Dissertation, University of Science and Technology of China, 49p. (in Chinese with English abstract).

Lin, G., 2015. Genesis of dolomites and its relationship with reservoirs in Dengying Formation in Gaoshiti-Moxi area, central Sichuan Basin. Master's Thesis, Southwest Petroleum University, Chengdu, 33p. (in Chinese with English abstract).

Lith, Y.V., Warthmann, R., Vasconcelos, C., Mckenzie, J.A., 2003. Microbial fossilization in carbonate sediments: a result of the bacterial surface involvement in dolomite precipitation. Sedimentology 50, 237–245.

Liu, S.G., Huang, W.M., Zhang, C.J., Zhao, X.F., Dai, S.L., Zhang, Z.J., Qin, C., 2008. Research status of dolomite genesis and its problems in Sichuan Basin. Lithologic Reservoirs 20 (2), 6–15.

Liu, H.J., Li, W., Zhang, B.M., Zhou, H., Yuan, X.H., Shan, X.Q., Zhang, J., Deng, S.W., Gu, Z.D., Fan, R., Wang, Y.J., Li, X., 2015. Sedimentary palaeogeography of the Sinian in Upper Yangtze Region. J. Palaeogeogr. 17 (6), 735–753.

Liu, J.L., Liu, K.Y., Li, C.W., Liu, W.J., 2020. Tectono-sedimentary evolution of the Late Ediacaran to early Cambrian trough in central Sichuan Basin, China: New insights from 3D stratigraphic forward modelling. Precambr. Res. 350, 1–20.

Liu, W., Qiu, N.S., Xu, Q.C., Liu, Y.F., 2018. Precambrian temperature and pressure system of Gaoshiti-Moxi block in the central paleo-uplift of Sichuan Basin, southwest China. Precambr. Res. 313, 91–108.

Liu, S.G., Song, J.M., Luo, P., Qing, H.R., Lin, B., Sun, W., Li, Z.W., Wang, H., Peng, H.L., Yu, Y.Q., Long, Y., Wan, Y.B., 2016b. Characteristics of microbial carbonate reservoir and its hydrocarbon exploring outlook in the Sichuan Basin, China. J. Chengdu Univ. Technol. (Sci. & Technol. Ed.) 43 (2), 129–152.

Liu, S.G., Wang, Y.G., Sun, W., Zhong, Y., Hong, H.T., Deng, B., Xia, M.L., Song, J.M., Wen, Y.C., Wu, J., 2016c. Control of intracratonic sags on the hydrocarbon accumulations in the marine strata across the Sichuan Basin, China. J. Chengdu Univ. Technol. (Sci. & Technol. Ed.) 43 (1), 1–23.

Liu, Q.Y., Zhu, D.Y., Jin, Z.J., Liu, C.Y., Zhang, D.W., He, Z.L., 2016a. Coupled alteration of hydrothermal fluids and thermal sulfate reduction (TSR) in ancient dolomite reservoirs: An example from Sinian Dengying Formation in Sichuan Basin, southern China. Precambr. Res. 285, 39–57.

Lu, K., Bao, Z.D., Sheng, M., Bao, Y.F., Dai, Q.Q., Cao, Y.Z., Liu, R., Zhang, S.C., Li, J., 2021. Influence of internal textures in fracture development in dolostones: A case study in the Mesoproterozoic Wumishan Formation in the Jizhong Depression, Bohai Bay Basin, north China. Mar. Pet. Geol. 125, 1–13.

Ma, Z.X., Luo, M.J., Liu, X.T., Ren, J.W., Huang, T., Sun, Z.M., 2019. Characteristics and genesis of the mixed siliciclastic-carbonate successions in the Upper Sinian Dengying Formation in the Nanjiang region. Sichuan. Sedimentary Geology and Tethyan Geology 39 (4), 1–13.

Marcos, F., Luiz, F.D.R., Carlos, H.L.B., 2009. Petrographic and seismic evidence for the depositional setting of giant turbidite reservoirs and the paleogeographic evolution of Campos Basin, offshore Brazil. Mar. Pet. Geol. 26, 824–853.

Mei, Q.H., He, D.F., Wen, Z., Li, Y.Q., Li, J., 2014. Geologic structure and tectonic evolution of Leshan-Longnvsi paleo-oplift in Sichuan Basin. China. Acta Petrolei Sinica 35 (1), 11–25.

Melnikov, N.V., Filiptsov, Y.A., Valchak, V.I., Simirnov, E.V., Borovikova, L.V., 2008. Petroleum potential of the Riphean-Vendian Chunya sedimentary basin in the western Siberian Platform. Russ. Geol. Geophys. 49, 176–182.

Meng, F.W., Ni, P., Schiffbauer, J.D., Yuan, X.L., Zhou, C.M., 2011. Ediacaran seawater temperature: Evidence from inclusions of Sinian halite. Precambr. Res. 184, 63–69.
Ni, Z.Y., Chen, Z.H., Li, M.J., Yang, C.Y., Wen, L., Hong, H.H., Luo, B., 2018. Trace element characterization of bitumen constraints on the hydrocarbon source of the giant gas field in Sichuan Basin, South China. Geol. J. 55 (1), 1–13.
Peng, J., 2010. The research of reservoir characteristics of the Dengying Formation in Southeast Sichuan. Chengdu University of Technology, Chengdu, p. 38p. Master's thesis,(in Chinese with English abstract.
Riding, R., 2000. Microbial Carbonates: the geological record of calcified bacterial-algal mats and biofilms. Sedimentology 47 (Suppl. 1), 179–214.
Riding, R., 2006. Microbial carbonate abundance compared with fluctuations in metazoan diversity over geological time. Sed. Geol. 185, 229–238.
Sánchez-Román, M., McKenzie, J.A., Wagener, A.D.L.R., Rivadeneyra, M.A., Vasconcelos, C., 2009. Presence of sulfate does not inhibit low-temperature dolomite precipitation. Earth and Planet. Sci. Lett. 285, 131–139.
Shemin, G.G., Chernova, L.S., Potlova, M.M., Vashchenoko, V.A., Doroginitskaya, L.M., Larichev, A.I., 2012. Key section of the Preobrazhenka productive horizon in the Vendian-Lower Cambrian carbonate complex (Lena-Tunguska petroliferous province). Russ. Geol. Geophys. 53, 175–184.
Shen, A.J., Zhao, W.Z., Hu, A.P., Wang, H., Liang, F., Wang, Y.S., 2021. The dating and temperature measurement technologies for carbonate minerals and their application in hydrocarbon accumulation research in the paleo-uplift in central Sichuan Basin, SW China. Petroleum Exploration & Development 48 (3), 476–487.
Shi, S.Y., Liu, W., Huang, Q.Y., Wang, T.S., Zhou, H., Wang, K., Ma, K., 2017. Dolostone reservoir characteristic and its formation mechanism in Qigebulake Formtion, Sinian, north Tarim Basin. Nat. Gas Geosci. 28 (8), 1226–1234.
Shi, Z.J., Peng, J., Wang, Y., 2010. Reservoir features and controlling factors of Dengying Formation in Southeast Sichuan, China. J. Chengdu Univ. Technol. (Sci. & Technol. Ed.) 37 (1), 1–8.
Shi, Z.J., Wang, Y., Tian, Y.M., Wang, C.C., 2013. Cementation and diagenetic fluid of algal dolomites in the Sinian Dengying Formation in southeastern Sichuan Basin. Sci. China: Earth Sci. 56, 192–202.
Słowakiewicz, M., Tucker, M.E., Pancost, R.D., Perri, E., Mawson, M., 2013. Upper Permian (Zechstein) microbialites: Supratidal through deep subtidal deposition, source rock, and reservoir potential. AAPG Bull. 97 (11), 1921–1936.
Song, J.M., Luo, P., Yang, S.S., Yang, D., Zhou, C.M., Li, P.W., Zhai, X.F., 2014. Reservoirs of Lower Cambrian microbial carbonates, Tarim Basin, NW China. Petroleum Exploration & Development 41 (4), 404–414.
Stefan, S., John, P.G., Joachim, E.A., Albert, M., 2005. Carbonate deposition and hydrocarbon reservoir development at the Precambrian-Cambrian boundary: The Ara Group in South Oman. Sed. Geol. 180, 1–28.
Tang, J.G., Hu, W.S., Li, W., Zhang, G.Y., 2013. Prediction of weathering paleokarst reservoirs by combining paleokarst landform with unconformity: A case study of Sinian Dengying Formation in Leshan–Longnüsi paleo-uplift, Sichuan Basin. Petroleum Exploration & Development 40 (6), 674–681.
Thomas, C.C., Michael, D.V.B., David, E.E., 2015. Petrography and characterization of microbial carbonates and associated facies from modern Great Salt Lake and Uinta Basin's Eocene Green River Formation in Utah, USA. Microbial Carbonates in Space and Time: Implications for Global Exploration and Production. Geol. Soc. Lond. Spec. Publ. 418, 261–286.
Tone, S., Lars, S., Snorre, O., 2018. Upper Permian carbonates at the northern edge of the Zechstein basin, Utsira High, Norwegian North Sea. Mar. Pet. Geol. 89, 635–652.
Wang, Y., 2006. Dolomite problem and Precambrian enigma. Adv. Earth Sci. 21 (8), 857–862.
Wang, D., 2010. Study on the Formation Mechanism of the High-quality Dolomite Reservoir of Dengying Formation in Nanjiang Area. Chengdu University of Technology, Chengdu, p. 36p. Master's thesis,(in Chinese with English abstract.
Wang, L., 2011. Reservoirs Characteristics and Distribution of Sinian Dengying Formation in Southeast Sichuan. Chengdu University of Technology, Chengdu, p. 40p. Master's thesis,(in Chinese with English abstract.
Wang, Z.C., Jiang, H., Wang, T.S., Lu, W.H., Gu, Z.D., Xu, A.N., Yang, Y., Xu, Z.H., 2014b. Paleo-geomorphology formed during Tongwan tectonization in Sichuan Basin and its significance for hydrocarbon accumulation. Pet. Explor. Dev. 41 (3), 305–312.
Wang, J., Li, Z.X., 2003. History of Neoproterozoic rift basins in South China: implications for Rodinia break-up. Precambr. Res. 122, 141–158.
Wang, G.Z., Liu, S.G., Liu, W., Fan, L., Yuan, H.F., 2014a. Process of hydrocarbon accumulation of Sinian Dengying Formation in Gaoshiti structure, Central Sichuan Basin, China. J. Chengdu Univ. Technol. (Sci. & Technol. Ed.) 41 (6), 654–693.
Wang, X.Z., Mu, S.G., Fang, S.X., Huang, J.X., Hou, F.H., 2000. Evolution of Porosity in the Process of Sinian Dolostone Diagenesis in Southwest Sichuan. Acta Sedimentol. Sin. 18 (4), 549–554.
Wang, W.Z., Yang, Y.M., Wen, L., 2016a. A study of sedimentary characteristics of microbial carbonate: A case study of the Sinian Dengying Formation in Gaomo area, Sichuan basin. Geology in China 43 (1), 306–318.
Wang, W.Z., Yang, Y.M., Zhang, X.H., 2016b. Reservoir characteristics and genesis of the Sinian Dengying Formation in Sichuan Basin. J. Northeast Petroleum Univ. 40 (2), 1–10.
Wood, R.A., Zhuravlev, A.Y., Sukhov, S.S., Zhu, M., Zhao, F., 2017. Demise of Ediacaran dolomitic seas marks widespread biomineralization on the Siberian Platform. Geology 45, 27–30.
Wu, J., Liu, S.G., Zhao, Y.H., Sun, W., Song, L.K., Song, J.M., Liang, F., Tian, Y.H., Long, Y., Li, J.L., 2014. Fluid characteristics of Upper Sinian-Lower Cambrian petroliferous strata in Gasoshiti-Moxi structure of Sichuan Basin, China. J. Chengdu Univ. Technol. (Sci. Technol. Ed.) 41 (6), 713–722.
Xie, K., Tan, X.C., Feng, M., Wang, B.B., Zhong, S.K., Yang, M.Y., Nie, W.C., Qiao, Z.F., Zeng, W., 2020. Eogenetic karst and its control on reservoirs in the Ordovician Majiagou Formation, eastern Sulige gas field, Ordos Basin, NW China. Petroleum Exploration and Development 47 (6), 1246–1261.
Xu, F.H., 2017. Fluid system and hydrocarbon accumulation of Sinian Dengying Formation and Cambrian Longwangmiao Formation in central Sichuan. Chengdu University of Technology, Chengdu, p. 101p. Doctoral Thesis,(in Chinese with English abstract.
Xu, H.L., Wei, G.Q., Jia, C.Z., Yang, W., Zhou, T.W., Xie, W.R., Li, C.X., Luo, B.W., 2012. Tectonic evolution of the Leshan-Longnüsi paleo-uplift and its control on gas accumulation in the Sinian strata, Sichuan Basin. Petroleum Exploration and Development 39 (4), 406–416.
Yuan, H.F., 2008. The Mechanism of Hydrocarbon Accumulation, Sinian-Lower Palaeozoic, Sichuan Basin. Chengdu University of Technology, Chengdu, p. 86p. Doctoral Thesis,(in Chinese with English abstract.
Yuan, H.F., Liu, Y., Xu, F.H., Wang, G.Z., Xu, G.S., 2014. The fluid charge and hydrocarbon accumulation, Sinian reservoir, Anpingdian-Gaoshiti Structure. Central Sichuan Basin. Acta Petrologica Sinica 30 (3), 727–736.
Zhao, D.F., Hu, G., Wang, L.C., Li, F., Tan, X.C., She, M., Zhang, W.J., Qian, B.F., Wang, X.F., 2020. Sedimentary characteristics and origin of dolomitic ooids of the terminal Ediacaran Dengying Formation at Yulin (Chongqing, South China). Palaeogeogr. Palaeoclimatol. Palaeoecol. 544, 1–13.
Zhao, Z.H., Li, L., Meng, Q.L., Jin, M.D., Zhang, Q., 2016. Sedimentary facies and evolution in Dengying formation of Sichuan basin. Geol. Surv. Res. 39 (4), 241–248.
Zhou, H., Li, W., Zhang, B.M., Liu, J.J., Deng, S.H., Zhang, S.B., Shan, X.Q., Zhang, J., Wang, X.B., Jiang, H., 2017. Formation and evolution of intraplatform basin from the late Sinian to early Cambrian in Sichuan Basin, China. Petroleum Res. 2, 41–53.
Zhou, Y., Yang, F.L., Ji, Y.L., Zhou, X.F., Zhang, C.H., 2020. Characteristics and controlling factors of dolomite karst reservoirs of the Sinian Dengying Formation, central Sichuan Basin, southwestern China. Precambr. Res. 343, 1–23.
Zhu, Z.P., Luo, W.J., Pan, R.F., Weng, X.B., Jin, J.N., 2019. The paleogeomorphology restoration of Sinian Deng 4 Member and its control on reservoir formation in the Gaoshiti-Moxi area in central Sichuan Basin. China Petroleum Exploration 24 (6), 730–738.
Zhu, G.Y., Zhang, S.C., Liang, Y.B., Ma, Y.S., Dai, J.X., Zhou, G.Y., 2006. Dissolution and alternation of the deep carbonate reservoirs by TSR: an important type of deep-buried high-quality carbonate reservoirs in Sichuan Basin. Acta Petrol. Sin. 22 (8), 2182–2194.
Zhu, D.Y., Zhang, D.W., Liu, Q.Y., He, Z.L., Li, S.J., Zhang, R.Q., 2015. Dynamic Development Process and Mechanism of Dolomite Reservoir under Multi-fluid Alternations. Nat. Gas Geosci. 26 (11), 2053–2062.